Abdominal Imaging

Published online: 22 November 2014

Abdom Imaging (2015) 40:1520–1557
DOI: 10.1007/s00261-014-0300-0

Primary biliary tract malignancies: MRI spectrum and mimics with histopathological correlation

Pardeep K. Mittal,[1] Courtney Coursey Moreno,[1] Bobby Kalb,[4] Ankush Mittal,[2] Juan C. Camacho,[1] Kiran Maddu,[1] Hiroumi D. Kitajima,[1] Brian C. Quigley,[3] Nima Kokabi,[1] William C. Small[1]

[1]Department of Radiology and Imaging Sciences, Emory University School of Medicine, 1365 Clifton Road NE, Building A, Suite AT-627, Atlanta, GA 30322, USA
[2]Emory University School of Medicine, Atlanta, GA 30322, USA
[3]Department of Pathology, Emory University School of Medicine, Atlanta, GA 30322, USA
[4]Department of Medical Imaging, University of Arizona, Tucson, AZ 85725, USA

Abstract

Contrast-enhanced magnetic resonance imaging and magnetic resonance cholangiopancreatography (MRCP), due to their excellent soft tissue contrasts, have become first-line noninvasive tests in the characterization and detection of both hepatic and pancreaticobiliary pathologies. MRCP is also helpful in detecting the level and cause of obstruction in patients presenting with jaundice. Cholangiocarcinoma (CCA) is the most common primary malignant tumor arising from the bile duct epithelium, with extrahepatic tumors presenting more often than with intrahepatic ones. However, the diagnosis and management of CCA is made more complex by a variety of malignant and benign conditions that resemble CCA, including hepatocellular carcinoma variants such as the fibrolamellar variant of hepatocellular carcinoma, cholangiocellular carcinoma, biliary metastases, hepatic inflammatory pseudotumor, lymphoepithelioma-like carcinoma, confluent fibrosis, primary sclerosis cholangitis, and the secondary sclerosing cholangitis complex. Consequently, knowledge of the underlying risk factors and imaging characteristics of these conditions is important in differentiating between neoplastic and non-neoplastic conditions in order to reach a definite diagnosis. Endoscopic retrograde cholangiopancreatography should be reserved for those patients who require intervention or biopsy for histopathological diagnosis.

Correspondence to: Pardeep K. Mittal; *email:* pmittal@emory.edu

Key words: Magnetic resonance imaging (MRI)—Cholangiocarcinoma (CCA)—Primary sclerosing cholangitis (PSC)

While there is a spectrum of intrahepatic and extrahepatic biliary conditions that ranges from neoplastic to non-neoplastic in nature, cholangiocarcinoma (CCA) is the most common primary biliary tract malignancy and the second most common primary hepatic malignancy, after hepatocellular carcinoma (HCC). Histologically, these CCAs are adenocarcinomas with profuse fibrous stroma arising from the bile duct epithelium and are observed in the entire biliary tree, in both intrahepatic and extrahepatic locations [1]. Historically, computed tomography (CT) and sonography have been used as noninvasive imaging techniques to evaluate biliary tract pathologies. CT offers high spatial resolution but limited soft tissue contrast and has the disadvantage of exposing the patient to ionizing radiation. Ultrasound (US) is widely used as an initial noninvasive imaging technique to evaluate suspected biliary tract obstruction. While US has some inherent advantages, including portability, cost, and the absence of radiation exposure, its limitations include operator dependency and limited imaging quality, preventing US from offering a definitive diagnosis. By comparison, magnetic resonance imaging (MRI) with magnetic resonance cholangiopancreatography (MRCP), in addition to high soft tissue contrast resolution, provides information regarding liver and biliary anatomy, the local extent of the tumor, extent of

ductal involvement, vascular involvement, and the presence of lymph nodes, liver metastases, and adjacent organ involvement. Endoscopic retrograde cholangiopancreatography (ERCP) also provides very important diagnostic information, complementary to MRCP findings, especially in the setting of suspected CCA. An approach to mimics of CCA with an emphasis on discriminators that can be used to help in narrow the differential diagnosis is summarized in Table 1.

MRI protocol

In our practice, we utilize a single abdominal MR imaging protocol including MRCP to evaluate nearly all gastrointestinal and solid abdominal pathologies, including biliary system pathologies. Our routine MRI protocol includes coronal and axial T1-weighted (T1W) 3D gradient echo (GRE) precontrast images with fat saturation; coronal and axial T2-weighted (T2W) single-shot fast spin echo (ssT2) images without fat saturation; axial ssT2 images with fat saturation; and T1-weighted 3D GRE dynamic axial contrast-enhanced images with fat saturation acquired in the arterial (timed through a bolus track method with breath-hold instructions triggered when the contrast bolus reaches the level of the diaphragm), portal venous (approximately 70 s delay), and delayed (axial 3-min delay and coronal 5-min delay) phases of enhancement. We also acquire axial dual echo gradient echo (in- and opposed-phases) images, steady-state free precession images, and heavily T2-weighted FSE MRCP images with all studies. Specific sequence parameters for abdomen MR imaging on a 1.5 T magnet are reported in Table 2. We administer gadobenate dimeglumine at a dose of 0.05 mmol per kg.

MRCP takes advantage of heavy T2 weighting to suppress all surrounding soft tissue, bone, and fat to focus on the biliary system. The single-shot 2D fast spin echo allows for acquisition without motion artifact despite a longer TR and TE. Without utilizing a single-shot method, respiratory navigation would be necessary to prevent this motion ghosting, as is commonly employed in 3D sequences. With a 3D technique, it may be advantageous to incorporate a variable flip angle to minimize specific absorption rate. The single-shot 2D technique is customarily acquired in the coronal and axial planes, and can be acquired as thick (40–60 mm) or thin (4–8 mm) slices.

Dynamic contrast-enhanced imaging is necessary to assess the enhancement properties of biliary pathology. For example, hyperenhancement during delayed imaging is characteristic of fibrous tissue, which is noted in large amounts in CCA and its mimics. In- and opposed-phase images are helpful for the identification of fat–water interfaces. In addition, susceptibility artifacts related to post-operative changes such as surgical clips or scar tissue and air typically demonstrate susceptibility artifacts on in-phase images acquired with longer echo times, especially in iatrogenic conditions. We use steady-state free precession images as a problem-solving sequence to evaluate the biliary and vascular systems, since this sequence is relatively insensitive to motion. In addition, contrast-enhanced MRI is able to demonstrate inflammation and neoplastic biliary wall changes, giving the added value of identifying biliary obstruction consequent to a variety of underlying malignant and benign conditions.

General approach to biliary conditions

When a biliary lesion is suspected or identified at imaging, the first step is to determine whether the lesion is intrahepatic or extrahepatic and to correlate with the clinical presentation, in particular the presence of jaundice. Morphology, signal characteristics, and the enhancement pattern of the lesions are helpful in narrowing the differential diagnosis of primary biliary lesions and their mimics. MR imaging characteristics of malignant strictures are summarized in Table 3.

Cholangiocarcinoma (CCA)

CCA is the most common primary biliary tract malignancy arising from the epithelial lining of both intrahepatic and extrahepatic ducts and was first reported by Durand and Fardel in 1840 [2]. Microscopically, 90% of CCAs are adenocarcinomas with abundant fibrous stroma [3, 4]. More men than women between the sixth and seventh decades of life are affected [5]. Currently, intrahepatic cholangiocarcinoma (ICC) accounts for 10–15% all primary liver cancers [6, 7] and for 3% of all GI cancers [8], but the incidence is on the rise. Risk factors of CCA are summarized in Table 4.

Anatomically, CCA is classified by location within the bile duct, with 10% of CCA presenting intrahepatically, 50% hilar (Klastkin tumor), and 40% in the distal bile duct [9, 10]. CCA of the proximal and distal bile ducts often present with features of obstructive jaundice, whereas ICC presents as a mass lesion in the absence of jaundice. The Liver Cancer Society of Japan describes three growth patterns of CCA: (1) mass forming, (2) periductal infiltrating, and (3) intraductal [3, 11].

MR imaging characteristics of morphological subtypes of CCA

Intrahepatic cholangiocarcinoma (ICC)

Mass-forming intrahepatic cholangiocarcinoma. The mass-forming type is the most common type of intrahepatic cholangiocarcinona (Fig. 1). More than 80% appear heterogeneous, and are accompanied by capsular retraction and satellite nodules, peripheral intrahepatic

Table 1. Cholangiocarcinoma mimics

Mimics	Discriminating features
Intrahepatic	
Hepatocellular carcinoma (HCC)-fibrolamellar	Young adults, median age 25 years Lack of known risk factors (e.g., chronic liver disease) T1 and T2 hypointense radial septa and central scar—post-contrast mild or partial enhancement of central scar or radial septa Central scar calcifications in 70% of patients Less vascular encasement or capsular retraction
Cholangiocellular carcinoma	Contains both elements of CCA and HCC T1 hypointense and T2 heterogenous Ring-like early arterial enhancement with progressive enhancement of central region over time Tissue biopsy for confirmation
Biliary metastases	History of primary neoplasm such as colorectal, breast, or lung carcinoma, etc. Colon carcinoma is the most common primary tumor metastasizing to biliary system, spreading along the epithelial lining T1 hypointense and T2 heterogenous Progressive delayed enhancement over time mimicking CCA Diagnosis based on history and histologic findings
Lymphoma	B cell lymphoma; symptoms of fever, abdominal pain, hepatomegaly Associated enlarged nodes and splenomegaly Post-contrast: uniformly enhancing tissue Less severe ductal obstruction compared to CCA Biopsy for confirmation and to guide treatment
Confluent fibrosis	Long-standing cirrhosis Wedge-shaped area with capsular retraction radiating from the porta hepatis apex Most common site: anterior segment of right hepatic lobe and medial segment of left hepatic lobe T1 hypointense and T2 hyperintense Uniform, delayed progressive enhancement of central region over time No biliary ductal obstruction or vascular invasion
Hepatic inflammatory pseudotumor	Patients present with fever, abdominal pain, jaundice Contains both T and B cells differentiating from lymphoma T1 hypointense and moderately T2 hyperintense Delayed progressive enhancement of central region over time Tissue biopsy for confirmation
Lymphoepithelioma-like carcinoma	Association Epstein–Barr virus T1 hypointense and T2 hyperintense Delayed progressive enhancement of central region over time Tissue biopsy for confirmation
Extrahepatic	
Primary sclerosing cholangitis (PSC)	Increased risk of development of cholangiocarcinoma (CCA) Association with inflammatory bowel disease MRI/MRCP: diffuse strictures and alternating dilatation giving beaded appearance involving both intra- and extrahepatic ducts Focal mass, bile duct stricture, and progressive biliary obstruction at serial imaging suggestive of development of CCA
AIDS cholangiopathy	Severely immunocompromised patients with CD4 count <100 mm^3 Severe epigastric pain and right upper quadrant pain Central intrahepatic ducts most commonly involved MRI: variable association with extrahepatic biliary abnormalities (such as papillary stenosis) and long extrahepatic bile duct strictures; intrahepatic pattern resembles PSC
Recurrent pyogenic cholangitis	Increased risk of CCA (2–6%) Repeated attacks of fever, abdominal pain, and jaundice Recurrent attacks of pyogenic cholangitis due to obstruction by pigment stones and biliary strictures MRI: biliary strictures, ductal wall thickening showing delayed enhancement secondary to fibrosis mimicking CCA, and pigment stones Lateral segment of left hepatic lobe and posterior segment of right hepatic lobe and extrahepatic ducts are most commonly involved
Autoimmune IgG4 cholangiopathy	Associated autoimmune sclerosing pancreatitis Clinical symptoms: obstructive jaundice High levels of plasma IgG4 in blood and histological specimens MRI: thick circumferential ring of enhancing tissue surrounding the stricture and narrowing of intrahepatic ducts and bile duct strictures with upstream ductal dilatation mimicking CCA Significant improvement after steroid administration.
Chemotherapy-induced biliary sclerosis	Hepatic artery infusion for chemotherapy Mechanism: drug-induced intravascular thrombosis and vasculitis MRI: strictures at bifurcation of common hepatic duct sparing distal duct

Table 1. continued

Mimics	Discriminating features
Post-traumatic sclerosing cholangitis	Ischemic changes due to arterial hypotension following severe trauma Involves intrahepatic ducts due to limited blood supply by peribiliary complexes MRI: stricturing and dilatation similar to PSC and potentially mimicking CCA
Iatrogenic (post-cholecystectomy) biliary strictures	History of cholecystectomy in 80% of cases Most common site of strictures: junction of cystic duct and common hepatic duct, also the confluence of right and left hepatic ducts Post-contrast MRI: progressive delayed enhancement of long-standing strictures
Ampullary/periampullary carcinoma	Presents like pancreatic head carcinoma Causes obstruction even if only a few mm in size and not apparent on imaging Marked and abrupt biliary or pancreatic duct dilatation Ampullary carcinoma of bile duct mimics distal duct CCA T1 hypointense and T2 hypointense Poor or moderate enhancement following contrast administration Tissue biopsy for confirmation
Mirizzi syndrome	Impacted stone in the gall bladder neck or cystic duct Narrowed common hepatic duct by extrinsic compression of stones Dilated intrahepatic ducts and common hepatic duct Subsequent inflammation around bile ducts causes stricture formation mimicking Periductal-infiltrating CCA

Table 2. MRI protocol

	Cor T2 SSFSE	Cor 3D T1FS GRE	Ax InOpp GRE	Ax T2 SSFSE	Ax T2 SPAIR SSFSE	Ax 3D T1FS GRE	Cor MRCP	Ax MRCP	Ax SSFP
TR	1500	3.98	175	1500	1500	3.85	4500	1500	3.07
TE	89	2.2	2.33, 4.99	83	83	2.15	756	682	1.54
FA	170	10	70	180	180	10	180	180	70
FOVr	380	400	360	380	380	350	300	300	380
FOVp	380	366	292	302	302	291	300	300	320
Nr	256	288	320	256	256	288	384	384	256
Np	256	172	182	184	184	168	269	269	216
ST	7	3	6	7	7	3	80	8	6
NEX	1	1	1	1	1	1	1	1	1
Slices	25	72	40	42	42	104	1	25	50
TA	37.5	15.46	31.98	63	63	17.76	1.63	4.05	22.5

SSFSE, Single-shot fast spin echo; GRE, Gradient echo; MRCP, Magnetic resonance cholangiopancreatography; SSFP, Steady-state free precession; TR, Repetition time; TE, Echo time; FA, Flip angle; FOVr, Read (frequency) field of view; FOVp, Phase field of view; Nr, Read (frequency) matrix; Np, Phase matrix; ST, Slice thickness; TA, Acquisition time; SPAIR, Spectral attenuated inversion recovery

Table 3. MRI and MRCP findings of malignant biliary strictures

High signal intensity relative to liver parenchyma on T2WI
Hyperenhancement relative to liver parenchyma on portal venous phase but showing progressive delayed enhancement
Length of strictured segment usually >12 mm
Wall thickness of strictured segment >5 mm
Indistinct outer margin
Luminal irregularity
Abrupt narrowing
Asymmetry

With permission from Kim et al. [115]

Table 4. Cholangiocarcinoma risk factors

Age >60 years
Males >females
Primary sclerosing cholangitis
Liver fluke infestation
Opisthorchis viverrini
Clonorchis sinensis
Caroli's disease
Choledochal cysts
Bile duct adenoma and biliary papillomatosis
Hepatolithiasis
Liver cirrhosis
Surgical biliary/enteric drainage procedures
Chemicals/agents, i.e., thorotrast, dioxin, vinyl chloride

With permission from Lazaridis and Gores [8]

ductal dilatation, and sometimes vascular encasement by the tumor, though typically without grossly visible tumor thrombus [12].

At MR imaging, intrahepatic mass-forming CCAs are hypointense on precontrast T1W imaging and hyperintense on T2W imaging, but are variable depending on the amount of fibrosis, necrosis, and mucin within the tumor [13]. Depending on the amount and distribution of tumor cells and fibrous tissue, four variable enhancement patterns have been noticed following contrast administration: (1) early arterial peripheral enhancement with progressive and concentric central filling with washout of periphery (most common) (Fig. 2), (2) early peripheral enhancement with a nonfilling central scar (Fig. 3), (3)

progressive complete enhancement (Fig. 4), and (4) complete early arterial hyperenhancement with subsequent washout on delayed phase (least common). As a result, in some cases, it may be difficult to distinguish between HCC and CCA on imaging, and tissue sampling may be required for definite diagnosis (Fig. 5) [14]. The most common pattern of enhancement of CCA is heterogeneous with progressive and prolonged delayed enhancement due to decreased arterial supply but abundant fibrous tissue and large interstitial spaces. Early enhancement and delayed washout corresponds to active growth of tumor cells. Partial or no filling of the central scar usually corresponds to an area of fibrosis, hyalinization, or necrosis. This classic pattern is not specific for CCA because it is seen most commonly in metastatic adenocarcinoma, but there are secondary signs associated with CCA including bile duct dilatation distal to the tumor, segmental or lobar atrophy with associated vascular encasement, capsular retraction, and a central scar [15, 16].

Periductal-infiltrating intrahepatic cholangiocarcinoma. Periductal-infiltrating ICC is characterized by growth along the bile ducts without mass formation; rather, there is diffuse periductal thickening and increased enhancement surrounding the dilated or narrowed ducts (Fig. 6). While peripheral ductal dilatation also can be noticed, it is rare in ICC and presents more frequently with hilar CCA. Early diagnosis of periductal-infiltrating CCA is difficult because the entity may look like benign strictures, but certain features are helpful in discriminating between benign strictures and true malignancy, such as long segmental strictures, irregular margins, asymmetric narrowing, ductal enhancement, lymph node enlargement, and periductal soft tissue lesions [12, 17].

Intraductal intrahepatic cholangiocarcinoma. Intraductal CCA presents with various patterns: (1) diffuse and marked ductal ectasia with or without a visible papillary mass (Fig. 7), (2) intraductal polyploid mass with ductal dilatation (Fig. 8), (3) intraductal cast-like lesions (Fig. 9), and (4) focal stricture with proximal ductal dilatation (Fig. 10). Intraductal ICC grows slowly and has a more favorable prognosis after surgical resection than other types of CCAs, so early diagnosis is important for patient survival. Intraductal ICC may be classified as either macroscopic or microscopic. Microscopic lesions are tumors with flat or micro papillary growth whereas macroscopic lesions manifest as papillary or tubular polyploid lesions [18].

Intraductal papillary mucinous neoplasms (IPMN) of the bile duct

Intraductal polypoid neoplasms of the biliary tract, known as intraductal papillary mucinous neoplasms (IPMNs) of the bile duct, are thought to be the counterpart of IPMNs of the pancreas due to their shared embryological development from the hepatic diverticulum in the foregut mesoderm [19]. These IPMNs mimic intraductal ICCs. IPMNs of the bile duct are tumors with numerous minute frond-like papillary projections and produce large amounts of mucin, which obstruct bile flow and causes severe biliary dilatation. At MRI, T2-weighted imaging demonstrates markedly dilated high signal duct with low-signal intra-luminal-filling defects. At MRCP, there is diffuse segmental aneurysmal dilatation of bile ducts with polypoid or nodular intraductal mass (Fig. 11).

Extrahepatic cholangiocarcinoma

Depending on its location, an extrahepatic cholangiocarcinoma may be classified as hilar cholangiocarcinoma (Klatskin tumor) or distal extrahepatic cholangiocarcinoma.

Hilar cholangiocarcinoma. Infiltrating type hilar cholangiocarcinoma is the most common type, accounting for approximately 70% of hilar cholangiocarcinomas [20]. These tumors can appear as mural thickening of the duct, soft tissue encircling the duct, or as a discrete mass. The most common finding is nonunion of the right and left hepatic ducts along with intrahepatic ductal dilatation and a normal-sized distal duct. The mass-forming exophytic hilar CCA and intraductal polypoid forms of hilar CCA are less common.

Distal extrahepatic cholangiocarcinoma. Distal extrahepatic cholangiocarcinomas may have varying degrees of presentation, including irregularity of the duct at the site of obstruction, a focal mass, or abrupt stricturing (shouldering), and, less frequently, intraductal papillary growth.

As these tumors are usually smaller and infiltrating, they are more homogeneous, and satellite lesions are less common due to early presentation because of ductal obstruction. Hilar and extrahepatic CCAs show MRI characteristics similar to those of ICC, such as T1 hypointensity and T2 hyperintensity with progressive delayed enhancement depending on the fibrous component. Hilar CCA (Fig. 12) and distal extrahepatic CCA (Fig. 13) are seen as abnormal circumferential extrahepatic ductal thickening and enhancement. However, duct wall enhancement alone may not be a predictor of a tumor as this can be seen in patients without tumor as a result of fibrosis or inflammation secondary to benign obstructive causes and/or subsequent stent placement. Therefore, MR imaging should be performed before any endoscopic procedure and or stent placement. Duct wall thickening of more than 5 mm has been suggested as an indicator of the presence of a tumor, but a high-grade

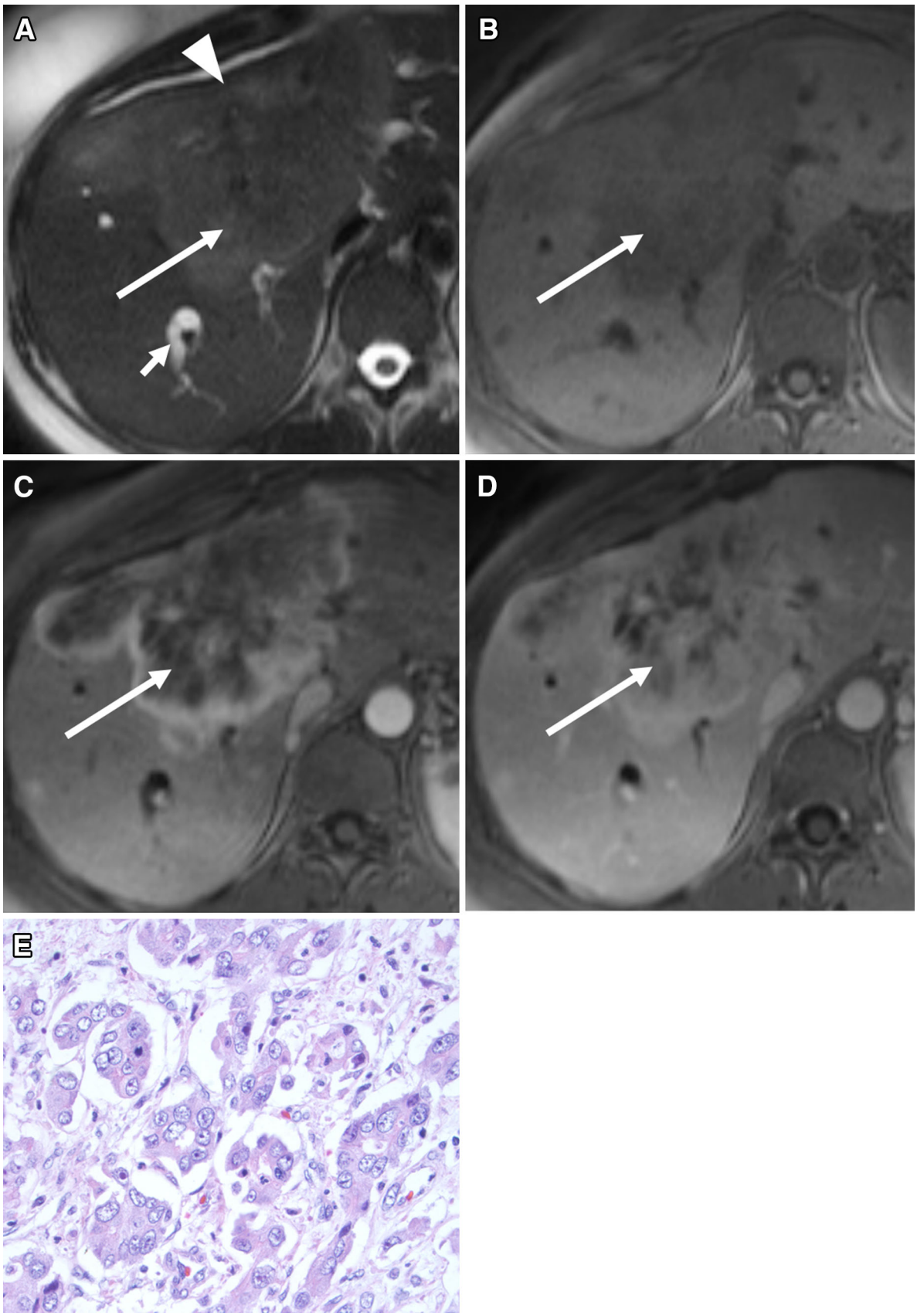
A
B
C
D
E

◀ **Fig. 1.** Classic intrahepatic cholangiocarcinoma: **A** Axial T2-weighted MR image demonstrating a mildly hyperintense mass (*arrow*) in segment 8 and 4A of the liver with associated capsular retraction (*arrowhead*) and subtle intrahepatic biliary dilation (*small arrow*) due to mass effect. **B** Precontrast T1-weighted image demonstrating a corresponding hypointense mass. **C** Arterial phase post-contrast axial MR image demonstrating a continuous ring of peripheral enhancement with central patchy areas of enhancement. **D** Delayed post-contrast axial MR image demonstrating progressive central enhancement. **E** Cholangiocarcinoma: small irregularly shaped tubules formed by cuboidal cells with crowded, large pleomorphic nuclei, pale chromatin, prominent nucleoli, and occasional mitotic figures (H&E ×400).

biliary obstruction, out of proportion with the degree of ductal wall thickening, may be a feature of CCA [21]. Distal extrahepatic CCA are frequently mistaken as adenocarcinomas of the pancreatic head [22]. Involvement of the intrapancreatic portion of the common bile duct without main or accessory pancreatic duct involvement suggests CCA instead of pancreatic adenocarcinoma.

Mimics of intrahepatic cholangiocarcinoma (ICC)

Hepatocelluar carcinoma (HCC)

Some variants of HCC may mimic CCA, such as the fibrolamellar variant of HCC and combined HCC and CCA (cholangiocellular carcinoma).

Fibrolamellar carcinoma

Fibrolamellar carcinoma (FLC) is a rare variant of HCC with distinct clinical, histopathological, and imaging features. It affects young adults with a median age of 25 years with a history of a lack of known risk factors,

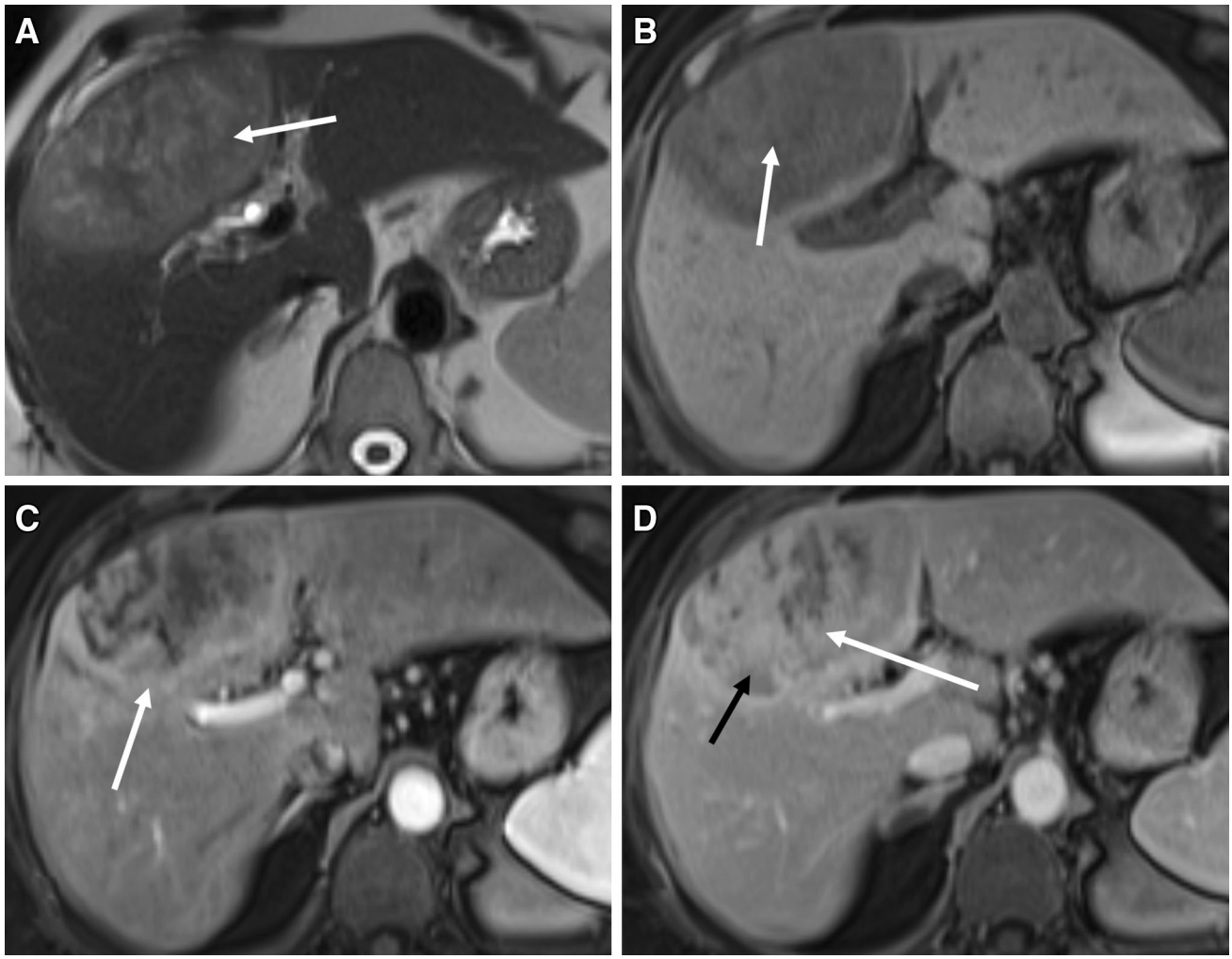

Fig. 2. Progressive concentric delayed enhancing mass-forming cholangiocarcinoma: **A** Axial T2-weighted MR image demonstrating a hyperintense mass (*white arrow*) in segment 8 and 4B of the liver. **B** Axial precontrast T1-weighted image demonstrating a corresponding hypointense mass (*arrow*). **C** Arterial phase post-contrast axial MR image demonstrating a peripheral rim of enhancement (*arrow*) relative to adjacent normal liver. **D** Delayed post-contrast axial MR image demonstrating progressive concentric central enhancement (*white arrow*) but peripheral rim showing washout (*black arrow*).

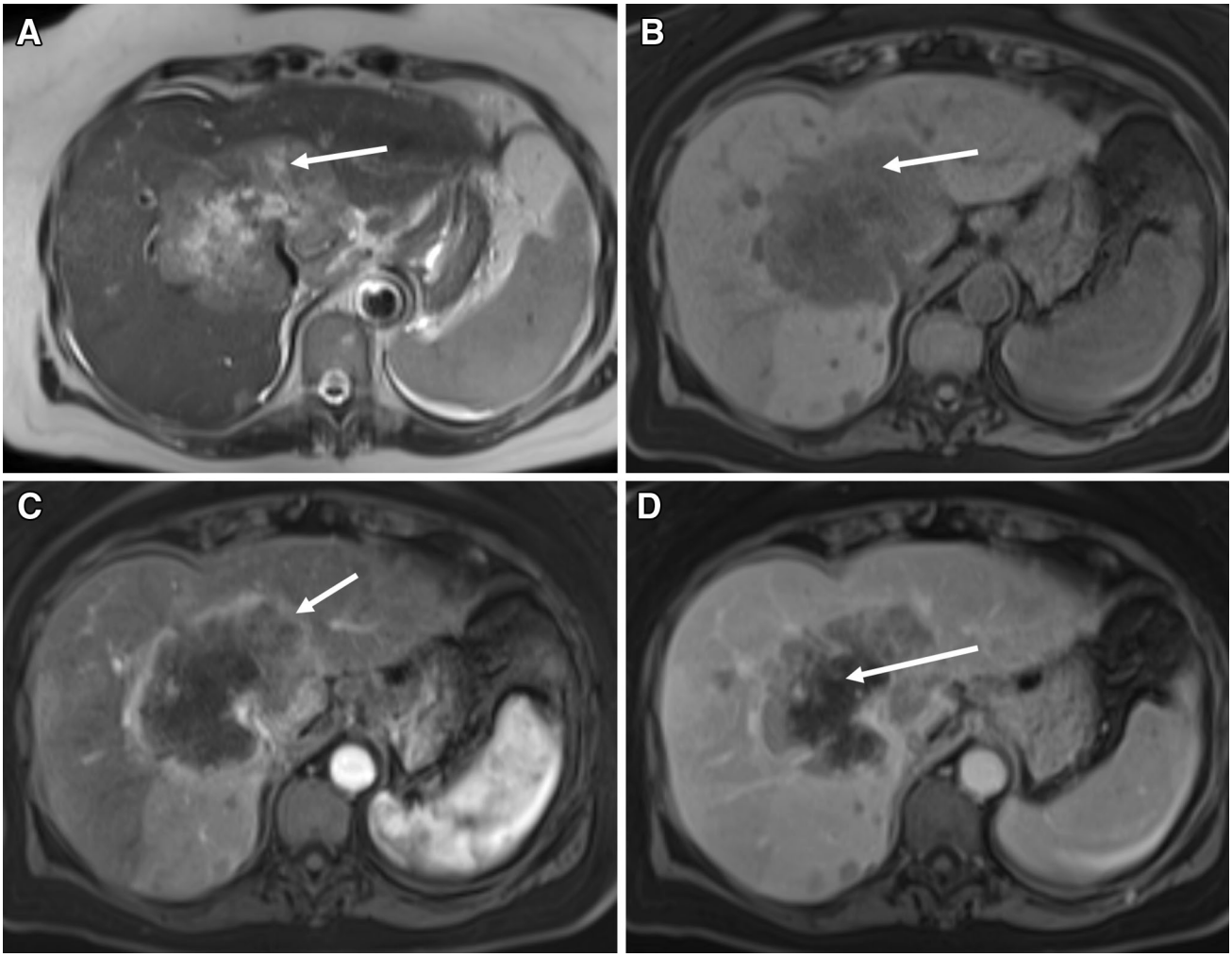

Fig. 3. Central nonenhancing mass-forming cholangiocarcinoma: **A** Axial T2-weighted MR image demonstrating a hyperintense mass (*arrow*) in segment 8 and 4A of the liver with associated large area of central necrosis. **B** Axial pre-contrast T1-weighted image demonstrating a corresponding hypointense mass (*arrow*). **C** Arterial phase post-contrast axial MR image demonstrating a hyperenhancing ring (*arrow*) relative to adjacent normal liver. **D** Delayed post-contrast axial MR image demonstrating patchy heterogeneous peripheral areas of enhancement. The core of the lesion does not show any significant contrast retention due to necrosis (*arrow*).

chronic liver disease, and elevated alpha-fetoproteins (AFP) [23]. FLC is less aggressive than classic HCC. Due to its indolent course, FLC often recurs as long as 5 years following resection. For unresectable patients, the median survival rate is 12 months [24].

At MR imaging, FLC tumors are T1 and T2 hypointense and show heterogeneous enhancement following contrast administration (Fig. 14). The majority of tumors are well defined/lobulated, and up to 70% show intratumoral calcification. While these calcifications are not as well seen on MRI as compared to CT (Fig. 14**E**), they rarely have a significant impact on diagnostic specificity. Uniformly T1 and T2 hypointense radial septa and a central scar in 70% of cases show mild or partial delayed enhancement in comparison to FNH, where the central scar is T2 hyperintense and shows delayed enhancement (Fig. 15) [25]. Intralesional fat has not been reported in FLC [26, 27]. Lymphadenopathy is present in 50% of patients at the time of presentation, especially in the hepatic hilum and hepatoduodenum ligament [28]. Capsular retraction and vascular invasion or encasement are less common in FLC, with 10% and 5% respectively, but they are common findings in CCA and HCC [27]. Histologically, FLC is characterized by well-differentiated large malignant hepatic cells with deep eosinophilic cytoplasm and macronucleoli surrounded by abundant fibrous bands [24, 29, 30].

Cholangiocellular carcinoma (combined hepatocellular and cholangiocarcinoma) (CLC)

Cholangiocellular carcinoma (combined hepatocellular and cholangiocarcinoma—CLC) is a rare form of pri-

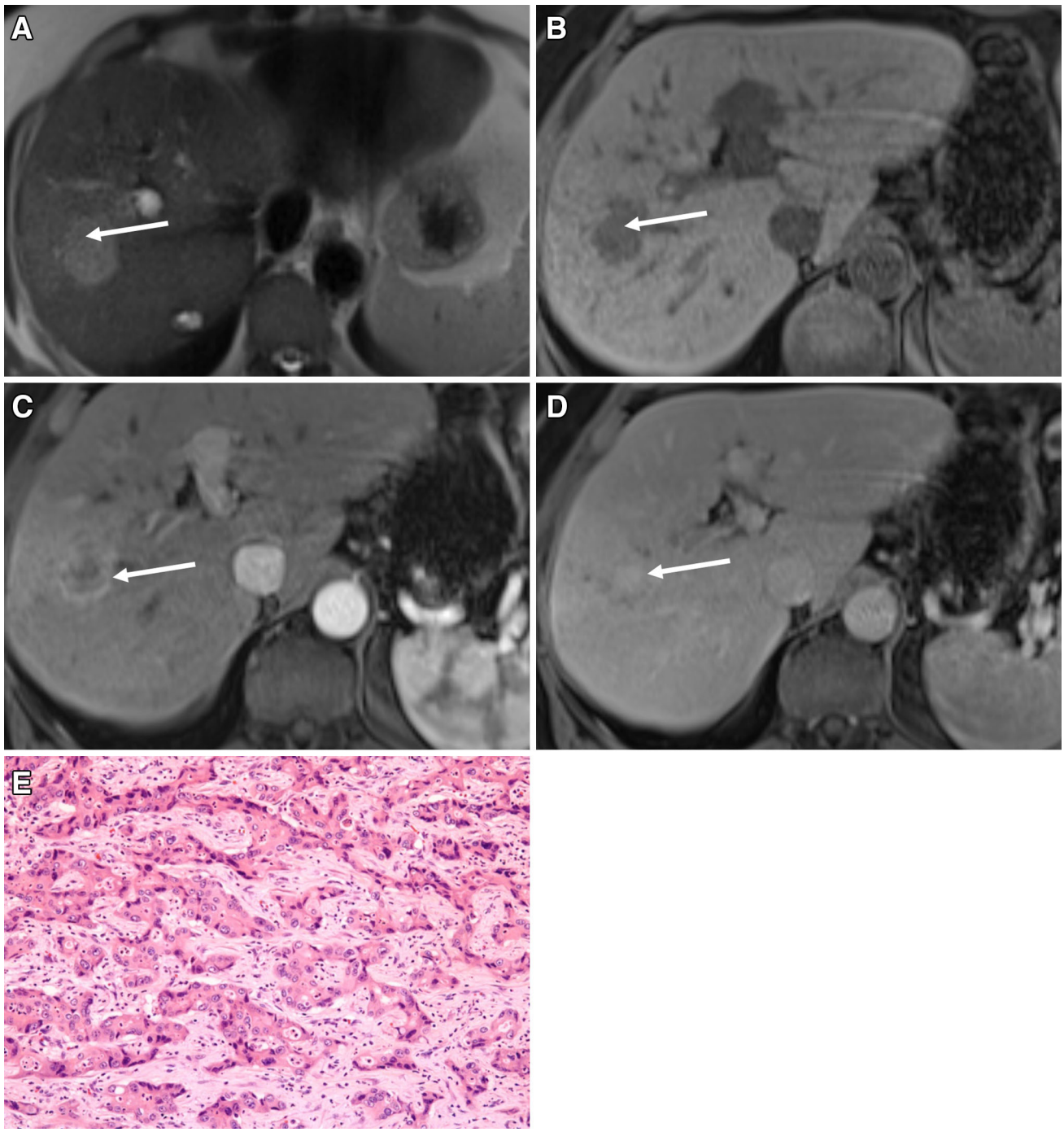

Fig. 4. Complete delayed centrally enhancing mass-forming cholangiocarcinoma**: A** Axial T2-weighted MR image demonstrating a hyperintense mass (*arrow*) in segment 8 of the right hepatic lobe. **B** Axial precontrast T1-weighted image demonstrating a corresponding hypointense mass. **C** Arterial phase post-contrast axial MR image demonstrating a lesion with avid peripheral hyperenhancement (*arrow*) relative to adjacent normal liver. **D** Delayed post-contrast axial MR image demonstrating delayed complete filling of the lesion**. E** Cholangiocarcinoma: irregular malignant glands, with infiltrative pattern and desmoplastic stroma (H&E ×100).

mary liver cancer, and accounts for approximately 1% of all primary liver tumors. CLC contains elements of both CCA and HCC in the same mass [31]. CLC originates from the hepatic progenitor cells present in most peripheral bile ducts (canals of Hering) [32]. Allen and Lisa classify CLC into three types: (1) a double cancer in which HCC and CCA exist separately, (2) a combined type in which HCC and CCA components exist contin-

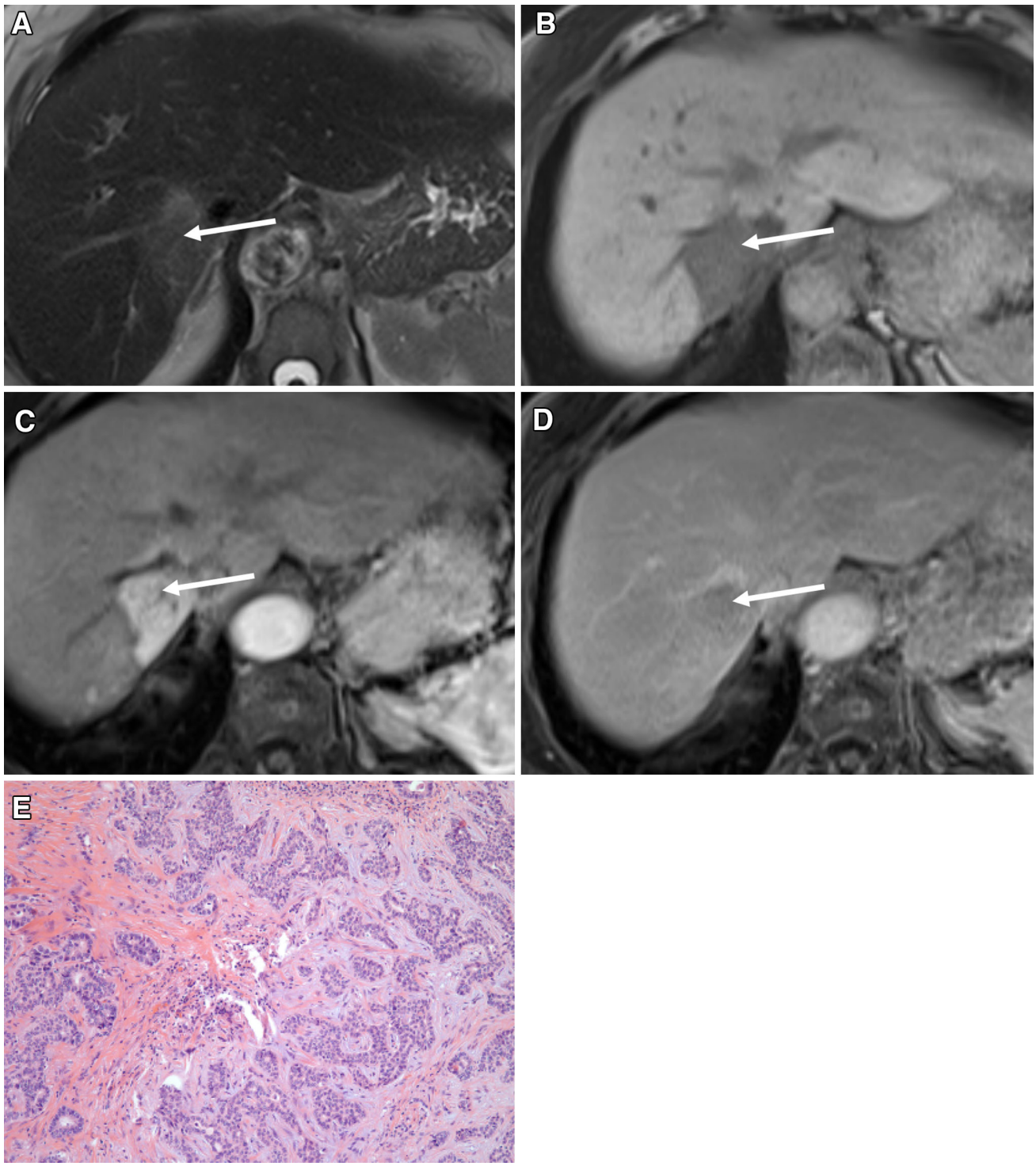

Fig. 5. Hypervascular mass-forming cholangiocarcinoma: **A** Axial T2-weighted MR image demonstrating a hyperintense mass (*arrow*) in segment 7 of the right hepatic lobe. **B** Axial precontrast T1-weighted image demonstrating a mass-like area of hypointensity. **C** Arterial phase post-contrast axial MR image demonstrating an avidly hyperenhancing lesion (*arrow*) relative to adjacent normal liver. **D** Delayed post-contrast axial MR image demonstrating washout. **E** Cholangiocarcinoma moderately differentiated, irregularly shaped, inter-anastomosing complex glandular structures infiltrate through a desmoplastic stroma (H&E ×200).

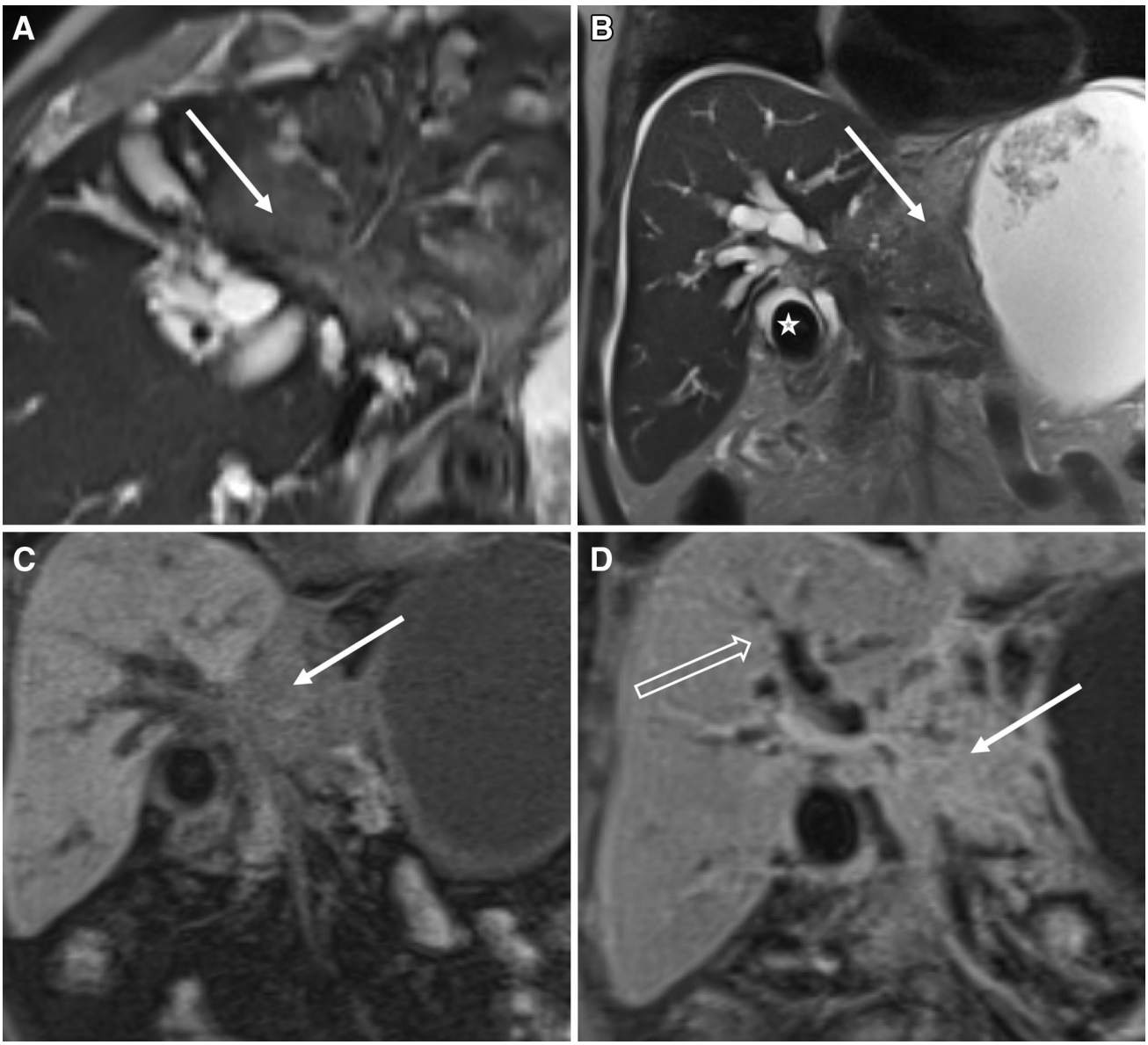

Fig. 6. Periductal infiltrative cholangiocarcinoma**: A** and **B** Axial and coronal T2-weighted MR images demonstrating an ill-defined periductal infiltrative hyperintense mass (*arrow*) in segments 2 and 3 of the left hepatic lobe with associated intrahepatic segmental areas of stenosis and dilation of the intrahepatic ducts. In addition, a large stone in the gallbladder neck is noted (*asterisk*). **C** Precontrast coronal T1-weighted image demonstrating a corresponding hypointense infiltrative mass (*arrow*). **D** Delayed post-contrast coronal MR image demonstrating a significant enhancing periductal soft tissue (*arrow*) as well as delayed periductal enhancement secondary to cholangitis due to ductal obstruction (*hollow arrow*).

uously but independently, and (3) a mixed type in which HCC and CCA are admixed within a mass [33].

At MR imaging, due to its mixed histopathological features, CLC shows dual imaging characteristics of both HCC and CCA. HCC-like early arterial enhancement and CCA-like persistent delayed enhancement, lack of necrosis or fibrous capsule, and peripheral location are characteristic imaging findings of CLC [32, 34, 35]. CLC is usually hypointense on T1WI and heterogeneously hyperintense on T2WI. On dynamic contrast-enhanced MRI, CLC most commonly displays early ring-like enhancement with central regions showing zero to minimal early enhancement but progressive enhancement over time (Fig. 16). Less commonly, CLC displays diffuse heterogeneous early enhancement with partial washout on delayed phase and with some areas of contrast retention. Definite diagnosis of CLC requires demonstration of both hepatocellular and cholangiocel-

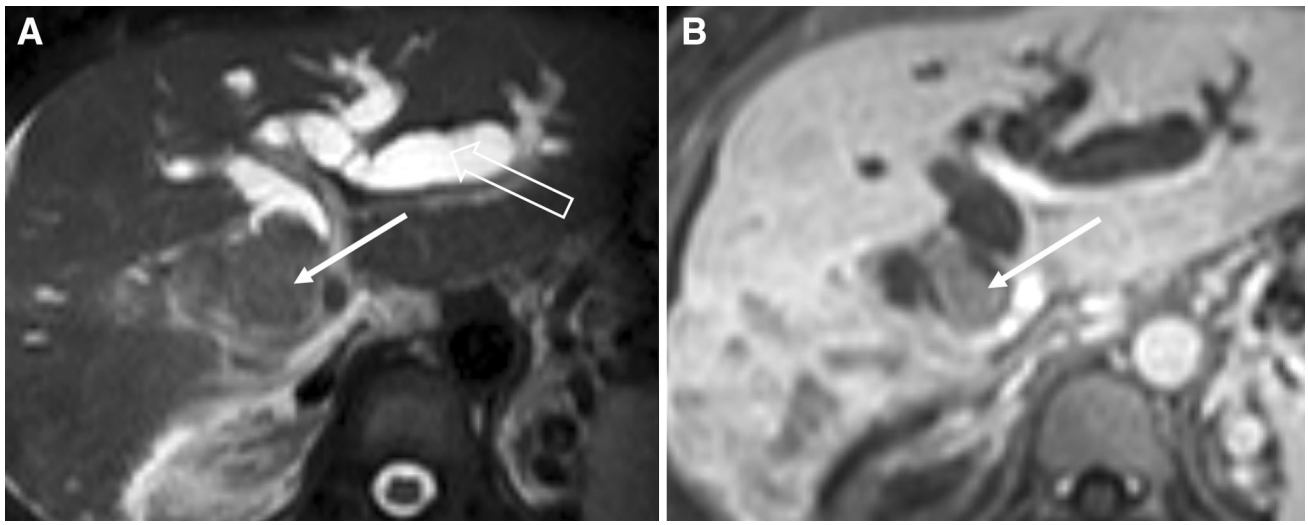

Fig. 7. Ductal ectasia with intraductal polypoid cholangiocarcinoma: **A** Axial T2-weighted MR image demonstrating ductal ectasia (*hollow arrow*) of the right and left intrahepatic ducts with a mildly hyperintense intraductal polypoid mass (*arrow*) within the right hepatic duct. **B** Post-contrast axial T1W image demonstrating a corresponding enhancing intraductal mass (*arrow*).

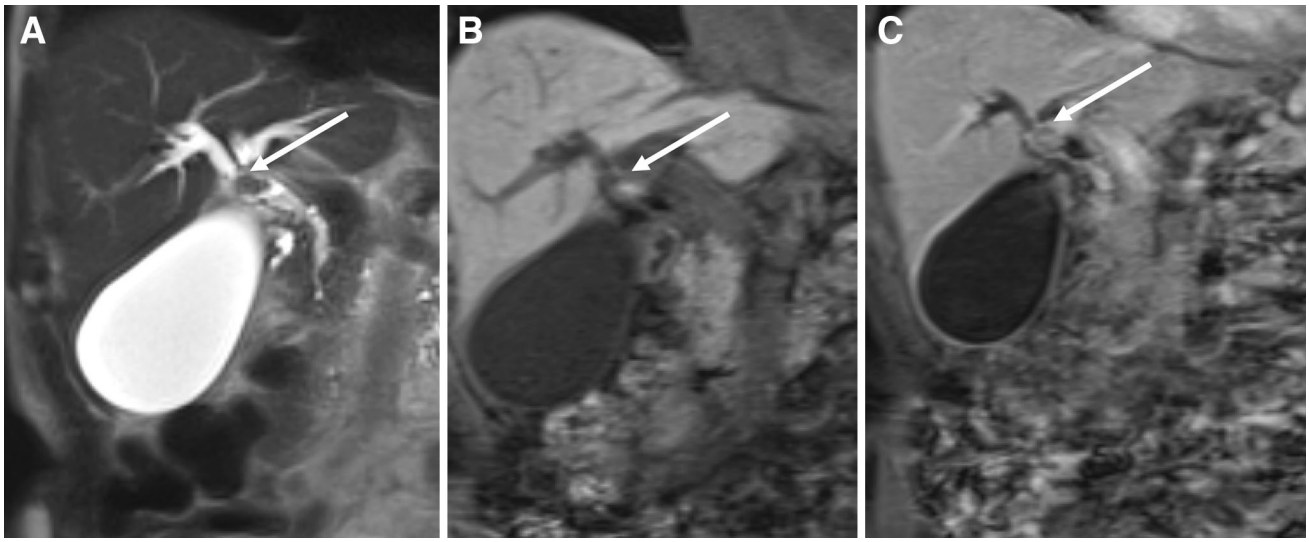

Fig. 8. Intraductal polypoid cholangiocarcinoma**: A** Coronal T2-weighted MR image demonstrating a mildly hypointense polypoid mass (*arrow*) relative to the liver parenchyma within the common hepatic duct. **B** Coronal precontrast T1-weighted image demonstrating a corresponding mildly T1 hyperintense mass (*arrow*). **C** Post-contrast coronal MR image demonstrating delayed enhancement of the mass (*arrow*).

lular differentiation at histopathology. Further, if diagnosis of CLC is suspected at imaging, the biopsy specimen should include an expanded volume of tumor, in order to increase the chances of sampling the interface area [36].

Biliary metastases

While intrabilary metastases are extremely rare, primary tumors that metastasize to the bile ducts are colon, breast, lung, gall bladder, melanoma, pancreas, and lymphoma. Colorectal carcinoma is the most common primary tumor to metastasize to the bile duct because of its propensity to spread along the epithelial lining and mimic other neoplasms, such as CCA in bile ducts (Fig. 17), transitional cell carcinoma in the bladder, and bronchialveolar carcinoma in the lungs [37, 38]. Several mechanisms have been postulated in the development of jaundice as related to the pattern of the spread of disease in patients with colorectal carcinoma: (1) parenchymal destruction by tumor nodules, (2) extrinsic compression by portal nodes, (3) infiltration of duct walls, and (4)

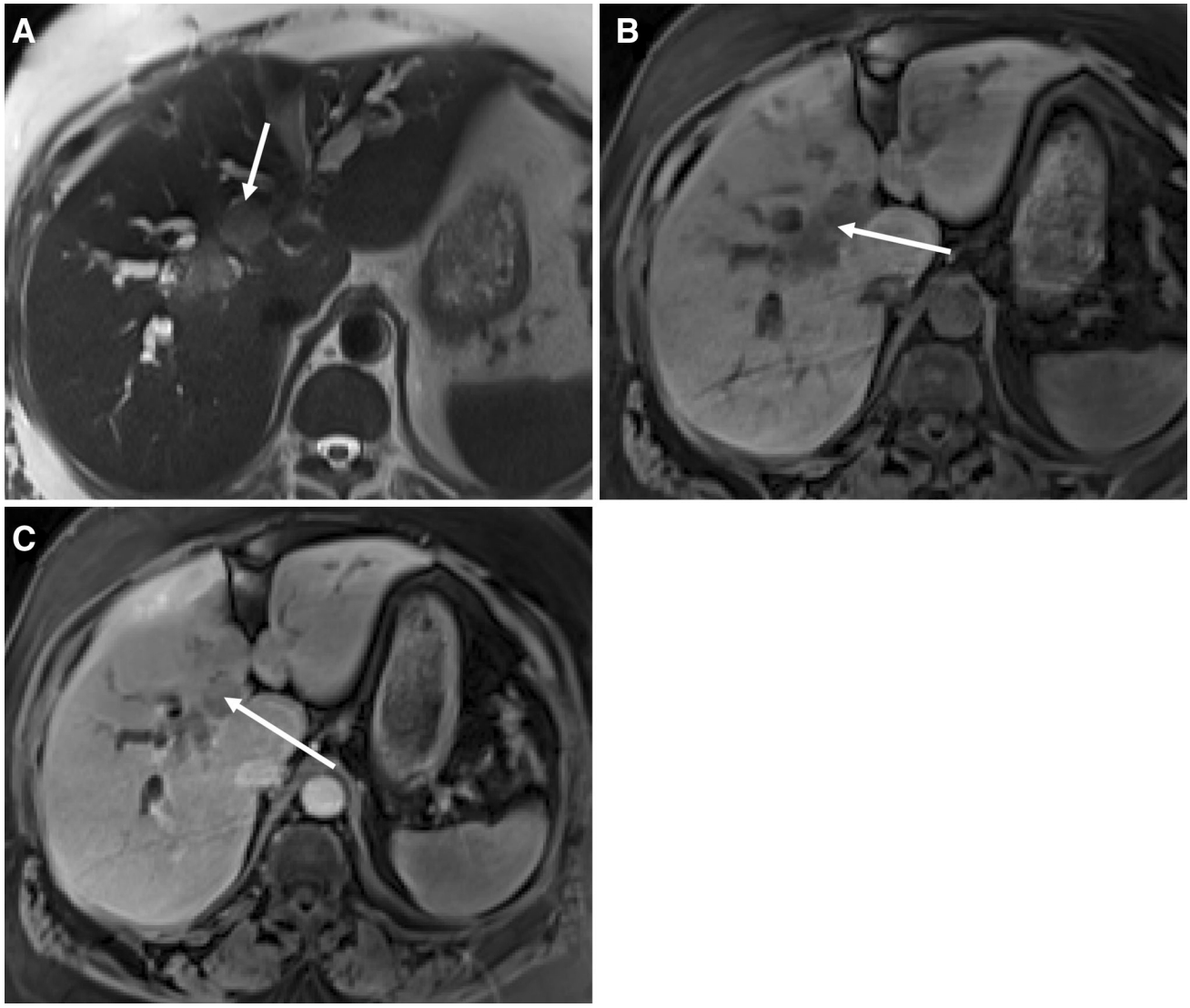

Fig. 9. Intraductal cast-like cholangiocarcinoma: **A** Axial T2-weighted MR image demonstrating a hyperintense intraductal cast-like mass within the dilated right and left hepatic ducts (*arrow*). **B** Axial precontrast T1-weighted image demonstrating a corresponding intraductal hypointense mass. **C** Delayed post-contrast MR image demonstrating heterogeneous delayed enhancement of the intraductal cast-like mass (*arrow*).

intrabiliary filling defects and luminal polyploid projections [38–41].

No imaging features allow for the distinction between colorectal metastases and CCA, because imaging findings may mimic all the three morphological forms of CCA [42]. PET scan is sensitive but not specific in differentiating colorectal carcinoma from CCA as increased FDG activity is seen in both. Consequently, diagnosis is based on histological findings and the patient's medical history. Immunochemistry is helpful in problem solving as tumor samples demonstrate cytokeratin 20 (CK20) positive and cytokeratin 7 (CK7) negative staining in colorectal carcinoma whereas CK7 is positive and CK20 is negative in bile duct epithelium carcinomas [43]. Distinction between primary and metastatic neoplasm is essential for management.

Primary biliary lymphoma

Primary lymphomatous involvement of the liver and biliary system, Hodgkin's or non-Hodgkin's, is extremely rare and usually a manifestation of systemic disease [44, 45]. Patients with hepatic lymphoma frequently present with B cell lymphoma symptoms such as fever, abdominal

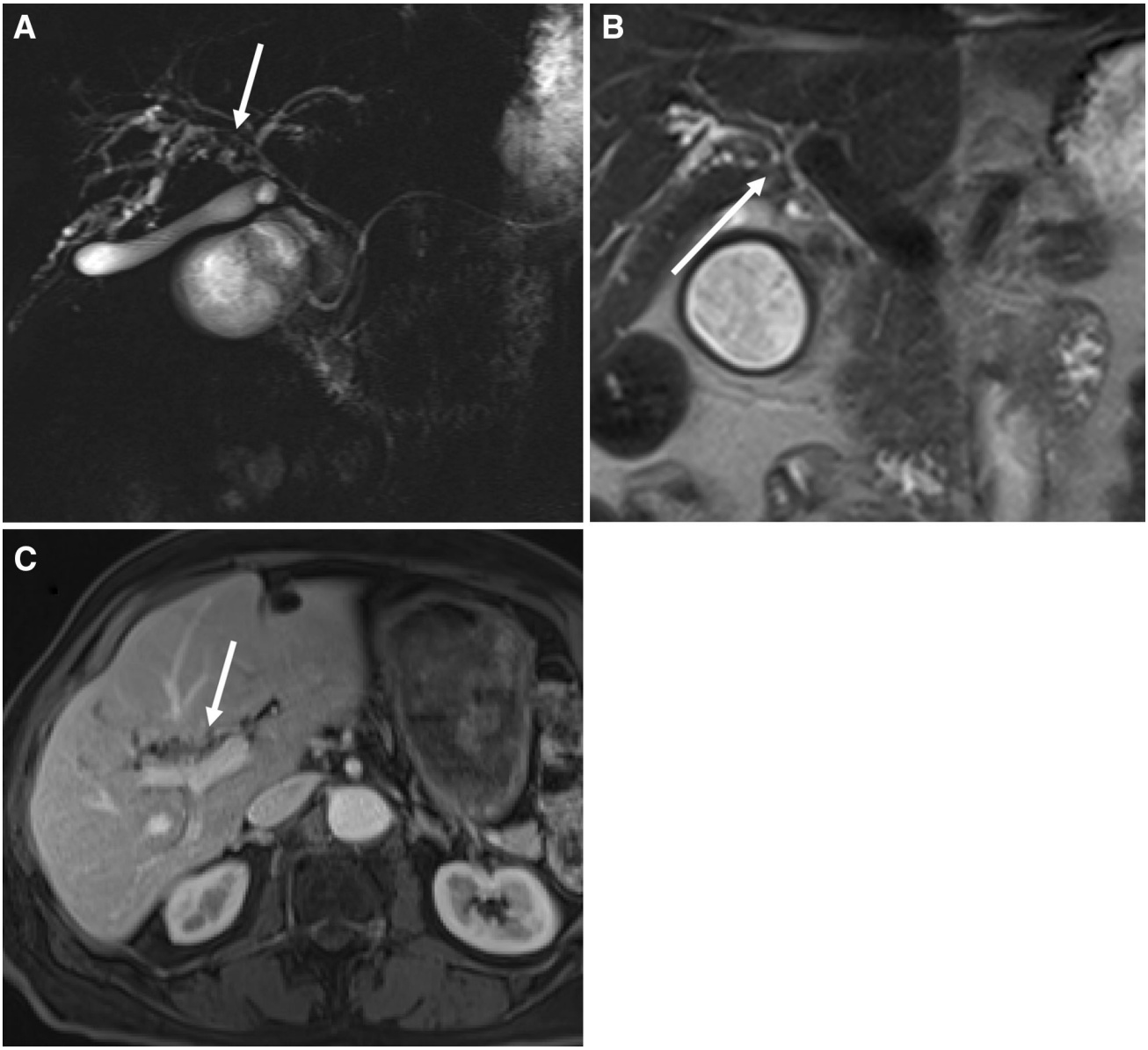

Fig. 10. Focal stricture as intraductal cholangiocarcinoma: **A** Coronal MRCP slab and **B** coronal T2-weighted MR image demonstrating focal stricture just above the confluence involving anterior branch of the right hepatic duct with associated upstream intrahepatic biliary ductal dilatation without a visible mass (*arrow*). **C** Delayed post-contrast axial MR image demonstrating an irregular appearance of the duct and periductal enhancement and focal area of stricture (*arrow*) without visible enhancing mass.

pain, and hepatomegaly. In addition, biliary tumors are generally accompanied by jaundice with evidence of biliary obstruction. The mechanism of jaundice in nodal lymphoma is compression of the extrahepatic ducts at the hepatic hilum, since the ducts are less mobile. On the other hand, enlarged nodes in the hepaticoduodenal ligament cause obstructive jaundice only if the duct is invaded; otherwise, the duct is displaced but not narrowed. The majority of primary hepatic lymphomas (90% of patients) are of the diffuse B cell type with a periductal spread pattern [46], while T cell lymphomas characteristically have a sinusoidal spread [47]. Primary lymphoma of the bile ducts was first described by Nguyen in 1982 as a localized thickening of extrahepatic bile ducts near the confluence with common hepatic duct involvement in patients presenting with jaundice, suggesting CCA (Fig. 18) [45].

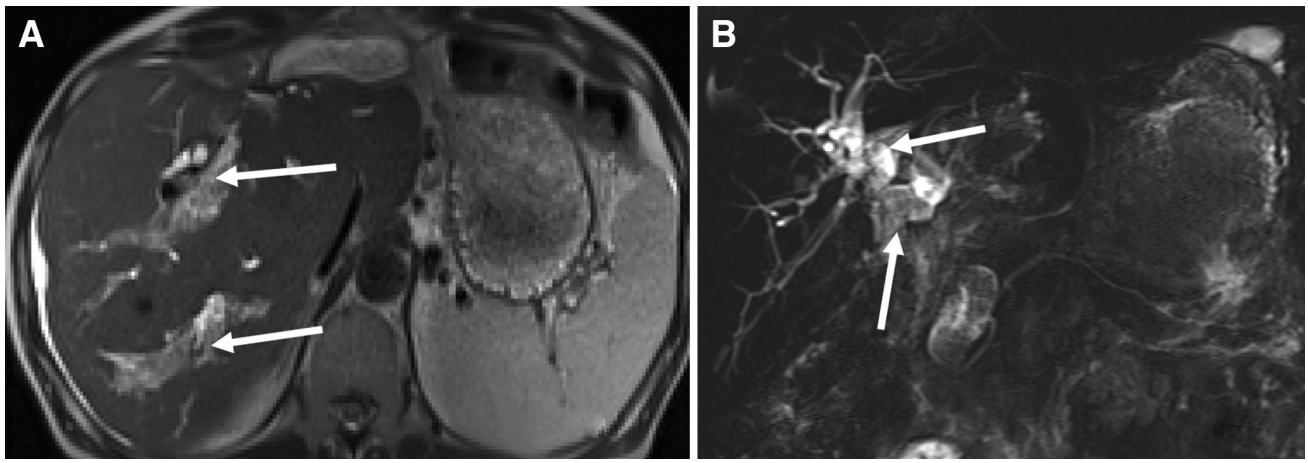

Fig. 11. Intraductal papillary mucinous neoplasm (IPMN) of the bile duct: **A** Axial T2-weighted MR image demonstrating a markedly dilated high signal duct with low-signal intra-luminal frond-like filling defects (*arrows*). **B** Coronal MRCP slab demonstrating diffuse segmental aneurysmal dilatation of bile ducts with polypoid mass (*arrows*).

Imaging of bile duct lymphoma, including strictures and soft tissue masses causing obstruction, is similar to CCA [45, 48]. Therefore, CCA and malignant lymphoma should be considered in the differential diagnosis of obstructive jaundice. Possible differentiating features on MRI include more uniformly enhancing tissue and less severe ductal obstruction with lymphoma compared to CCA. In addition, lymphoma demonstrates markedly elevated restricted diffusion on DWI, while CCA may only demonstrate mild diffusion restriction. Finally, association of biliary tumor with markedly enlarged lymph nodes and splenomegaly suggests lymphoma as the primary diagnostic consideration. As management is different in each case, biopsy should be strongly considered in difficult cases to establish a definite histopathological diagnosis before surgical treatment.

Confluent hepatic fibrosis

Confluent hepatic fibrosis commonly occurs in the context of long-standing cirrhosis as a result of hepatic parenchymal collapse and its replacement with fibrotic masses. It appears as a wedge-shaped area with overlying capsular retraction radiating from the porta hepatis apex. It most commonly involves the anterior segment of the right hepatic lobe and the medial segment of the left hepatic lobe. At MR imaging, the fibrosis appears as low signal intensity on precontrast T1WI and high signal intensity on T2WI and shows a geographic pattern. Postcontrast imaging demonstrates persistent progressive delayed enhancement [49, 50], similar to delayed contrast retention due to fibrous stroma in CCA, but one can differentiate confluent fibrosis from CCA on the basis of no surrounding biliary ductal dilatation or adjacent vascular invasion (Fig. 19) [49, 51].

Hepatic inflammatory pseudotumor (IPT)

Hepatic inflammatory pseudotumor (IPT), also known as inflammatory myofibroblastic tumor, is a rare benign process most commonly involving the lungs and orbits in young adults, especially in Asia [52, 53]. Hepatic IPT was first described by Pack and Baker [54], and is an uncommon disorder that sometimes mimics a malignant tumor, CCA, or metastatic disease [55]. Patients usually present with fever, abdominal pain, and jaundice. The etiology of IPT is unknown, but occlusive phlebitis, biliary obstruction, or undetected infectious agents are possible causes [56].

Histologically, IPT is characterized by acute and chronic inflammation consisting of lymphocytes, plasma cells, histiocytes, myofibroblastic spindle cells, and collagen/fibroblasts [57–59]. There are three subtypes of IPT: (1) xanthogranuloma type pseudo tumor, (2) plasma cell granuloma type pseudo tumor, and (3) sclerosing pseudo tumor [56]. Both T and B cells are present in IPT, differentiating IPT from lymphoma, where clonal population of either T or B cells is present [58]. EBV could be an etiological factor in these lesions [60]. Spontaneous regression of hepatic IPT has been noticed. The imaging features of hepatic IPT are nonspecific—they can manifest as single or multiple masses and they usually involve not only the right hepatic lobe, but also the porta hepatis and bile ducts in rare cases, causing obstructive jaundice. At MR imaging, hepatic IPT is hypointense on precontrast T1WI and hyperintense on T2WI and demonstrates persistent progressive delayed enhancement due to fibrous tissue, similar to CCA (Fig. 20). IPT may be associated with recurrent pyogenic cholangitis, leading to stricture formation in the intrahepatic and extrahepatic ducts and mimicking periductal infiltrating CCA [61, 62]. IPT poses both a clinical and a radiological challenge

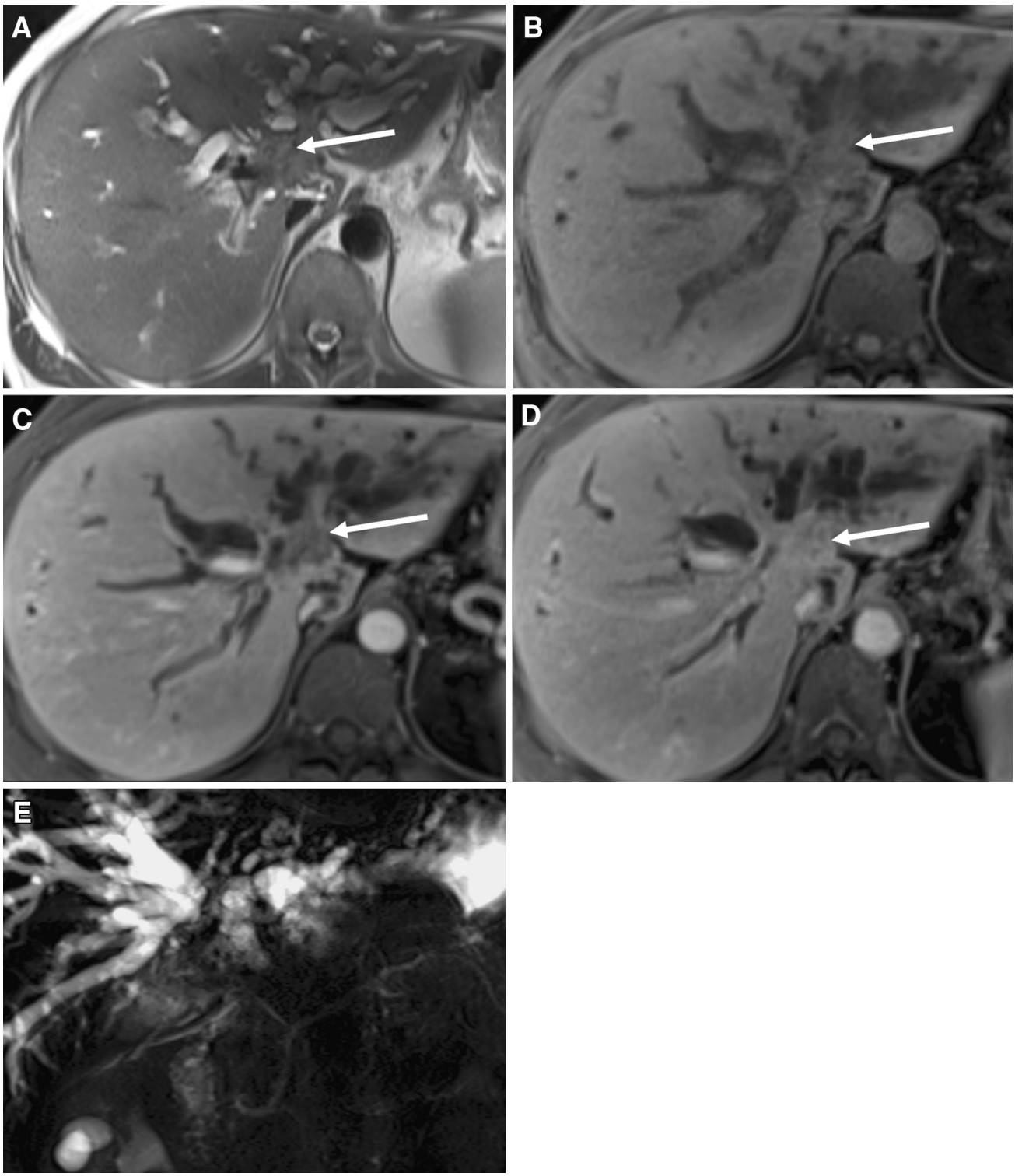

Fig. 12. Periductal infiltrative hilar cholangiocarcinoma (Klatskin's tumor)**: A** Axial T2-weighted MR image demonstrating a mildly hyperintense infiltrative hilar mass (*arrow*) predominantly in segment 4B with extension into the periductal soft tissues of segment 3. **B** Precontrast axial T1-weighted image demonstrating a corresponding infiltrative hypointense mass (*arrow*). **C** Arterial phase post-contrast axial MR image demonstrating a continuous ring of peripheral enhancement surrounding the mass (*arrow*). **D** Delayed post-contrast axial MR image demonstrating progressive enhancement relative to the surrounding liver parenchyma (*arrow*). **E** On coronal MRCP slab, the mass isolates the common left hepatic duct from the confluence of the anterior and posterior right ducts.

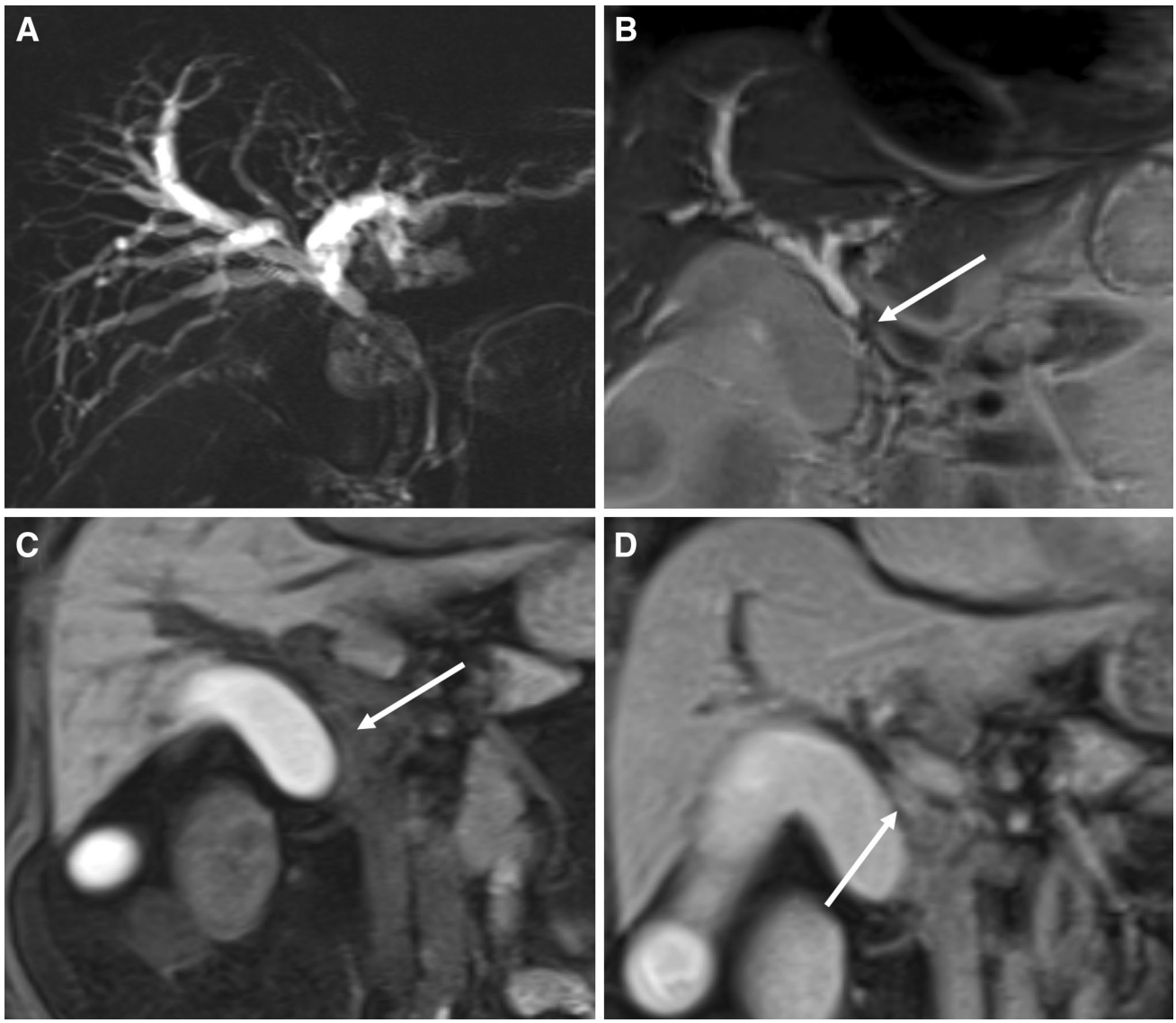

Fig. 13. Distal extrahepatic cholangiocarcinoma: **A** Coronal MRCP slab demonstrating distal common bile duct stricture with upstream biliary ductal dilatation. **B** Coronal T2-weighted MR image demonstrating a hypointense mass (*arrow*) involving the distal duct. **C** Coronal T1-weighted precontrast image demonstrating the corresponding low signal (*arrow*). **D** Delayed post-contrast coronal image demonstrating progressive enhancement of soft tissue mass involving the distal duct (*arrow*).

because of its clinical similarity to malignant tumors, such as CCA, and its nonspecific imaging characteristics. Therefore, a needle biopsy is required for a correct diagnosis; recognition of IPT in a patient can prevent unnecessary surgery since the patient can be treated with antibiotics, steroids, and chemotherapeutic agents [63].

Lymphoepithelioma-like carcinoma (LELC)

Lymphoepithelioma is an undifferentiated carcinoma in the nasopharynx originally described by Regaud and Schminke [64] and is characterized by intense lymphoid plasmacytoid stroma [65, 66]. Lymphoid stroma-rich carcinomas in other organs have been described as LELCs. In the hepatobiliary tract, primary LELCs are extremely rare and are reported as case reports only, identified as LELC, similar to CCAs [67]. Epstein–Barr virus (EBV) plays an important role in the pathogenesis of LELCs [67], but there are case reports in the literature that lack an EBV association. The mass is hypointense on precontrast T1WI and slightly hyperintense on T2WI. Dynamic contrast-enhanced imaging shows progressive delayed enhancement (Fig. 21) [65]. Shirabe et al. [68]

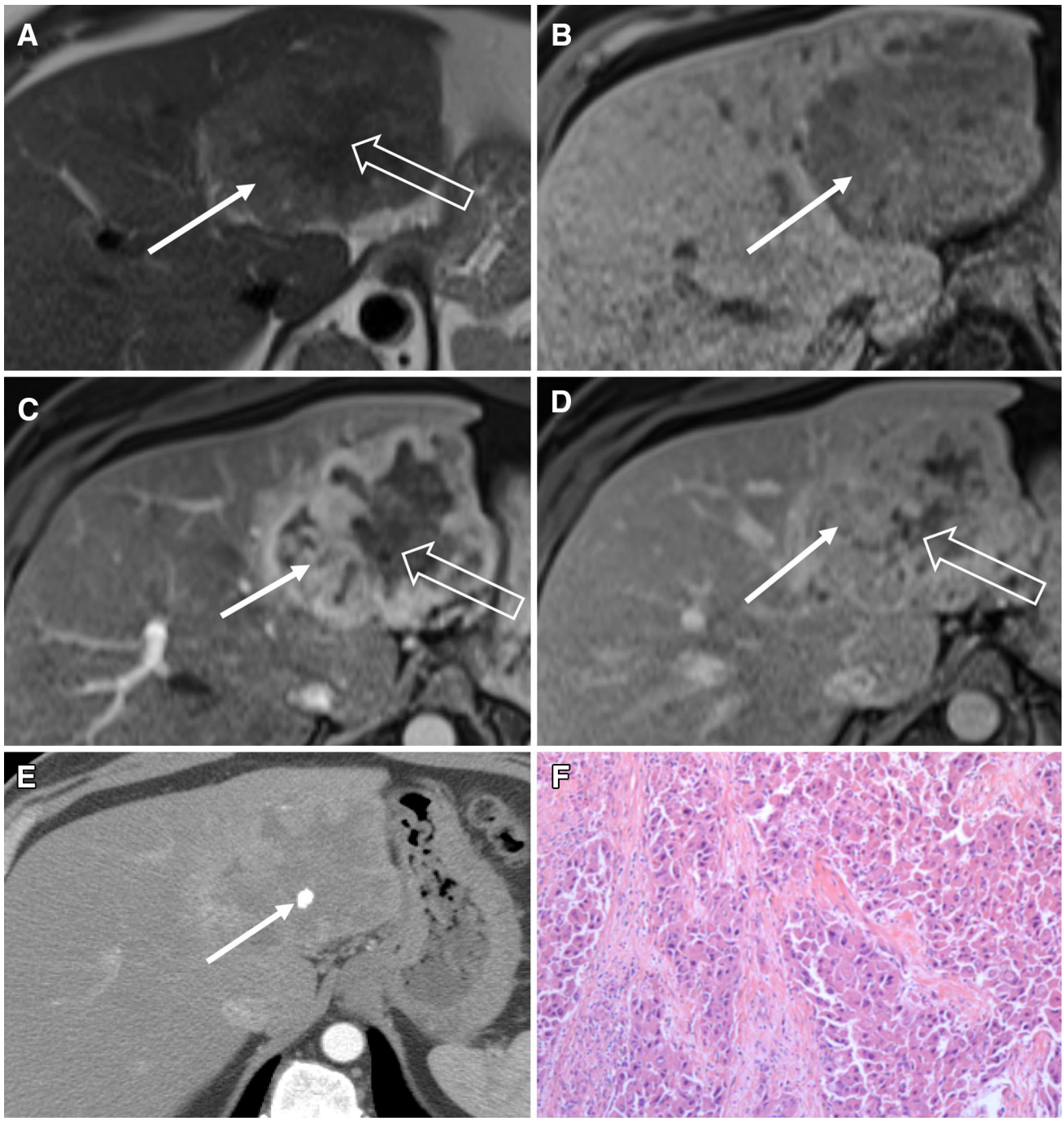

Fig. 14. Fibrolamellar type of hepatocellular carcinoma: **A** Axial T2-weighted image demonstrating a hyperintense lesion (*arrow*) with a hypointense central scar (*hollow arrow*). **B** Axial T1-weighted precontrast image demonstrating the corresponding low signal (*arrow*). **C** Arterial phase showing a heterogeneous enhancement of the mass (*arrow*) but no enhancement of central scar (*hollow arrow*). **D** Delayed postcontrast image demonstrating progressive enhancing mass (*arrow*) but partially enhancing central scar (*hollow arrow*). **E** CT scan demonstrating calcifications in the central scar (*arrow*). **F** Fibrolamellar carcinoma: relatively parallel fibrous bands course throughout the tumor, which is composed of neoplastic hepatocytes with abundant granular eosinophilic cytoplasm (H&E $\times$200).

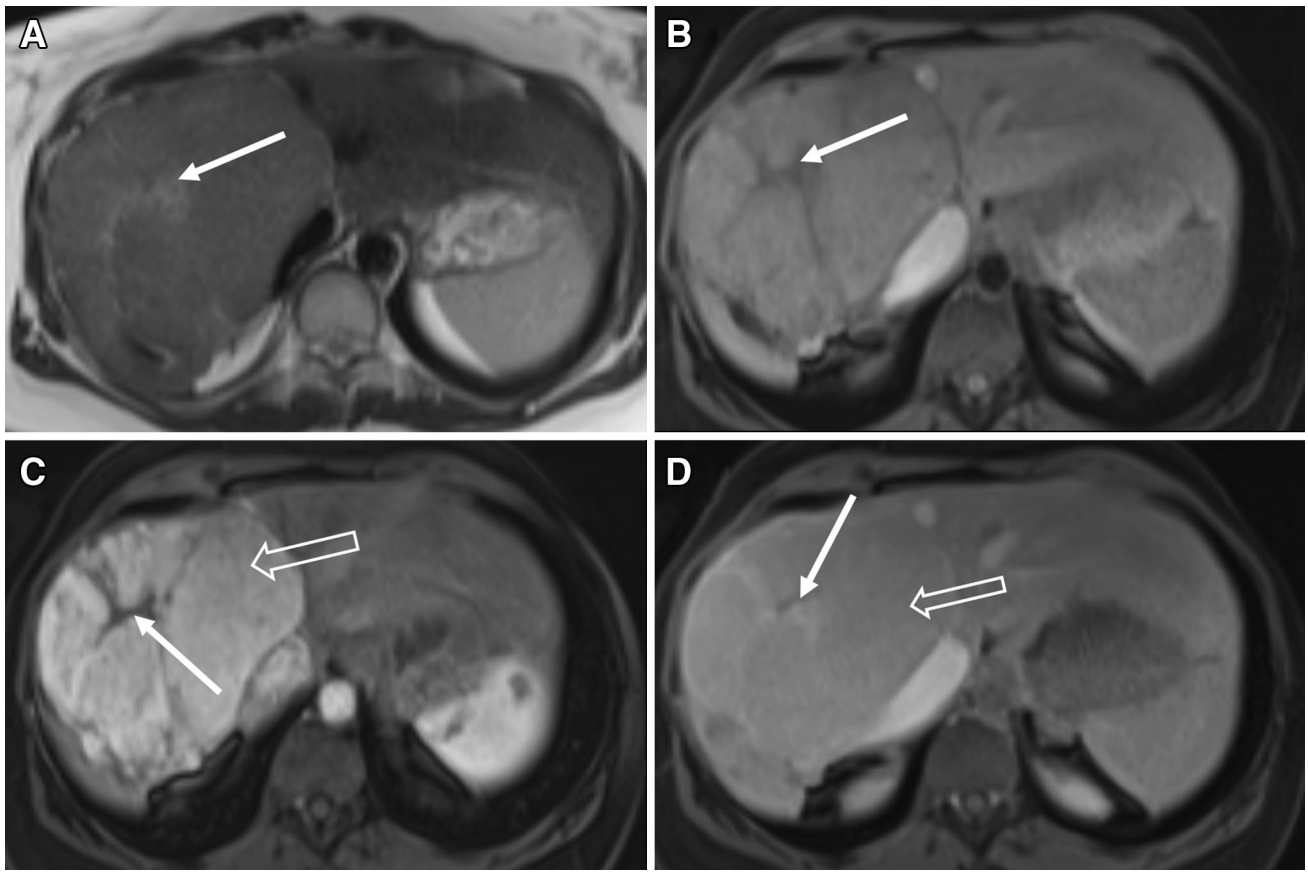

Fig. 15. Focal nodular hyperplasia: **A** Axial T2-weighted image demonstrating a slightly hyperintense lesion with a hyperintense central scar (*arrow*). **B** Precontrast axial T1-weighted image demonstrating a corresponding isointense mass but hypointense central scar (*arrow*). **C** Arterial phase show avidly enhancing mass (*hollow arrow*) but no enhancement of central scar (*arrow*). **D** Delayed post-contrast image demonstrating a mass becoming isointense to liver (*hollow arrow*) but central scar demonstrates hyperenhancement (*arrow*).

reported a case of HCC with lymphoid stroma and suggested a distinct category with a favorable prognosis [69]. This category was later described as LELC-HCC by Emile et al. [70].

Mimics of extrahepatic cholangiocarcinoma

Primary sclerosing cholangitis (PSC)

PSC is a chronic cholestatic disorder of the liver characterized by progressive inflammation and fibrosis of the intrahepatic and extrahepatic bile ducts, leading to multifocal stricture formation and eventual end-stage liver disease. PSC is likely immune mediated, but the exact etiology remains unclear. It is most common in men with an average age of 42 years [71]. The most dreaded complication of PSC is the development of CCA, with a reported incidence of 0.6–1.5% per year [72, 73]. The highest incidence is in the first 2 years after diagnosis of PSC. CCA in patients with PSC develops three decades earlier than in patients without PSC [73]. Also, there is a well-established association between inflammatory bowel diseases, most commonly ulcerative colitis (UC) which is present in 60–80% of patients with PSC. In patients with both PSC and UC, there is a higher risk of development of colon cancer than in patients with UC alone, so it is recommended that all patients with PSC and IBD should be placed on aggressive surveillance with colonoscopy with random biopsies at least every 2 years from the diagnosis of PSC [74, 75].

Historically, ERCP has been considered the gold standard in the diagnosis of PSC [76]. However, ERCP is an invasive procedure that is associated with the risk of acute pancreatitis and cholangitis, while MRI with MRCP is a noninvasive procedure and an alternative to ERCP that can be used in the initial work up. At imaging, diagnosis of PSC is established by demonstration of diffuse strictures and alternating dilatation giving the classic beaded appearance involving both the intra- and extrahepatic ducts (Fig. 22). Small duct PSC is histologically consistent with PSC in the setting of a normal cholangiogram and has a favorable prognosis [71, 77].

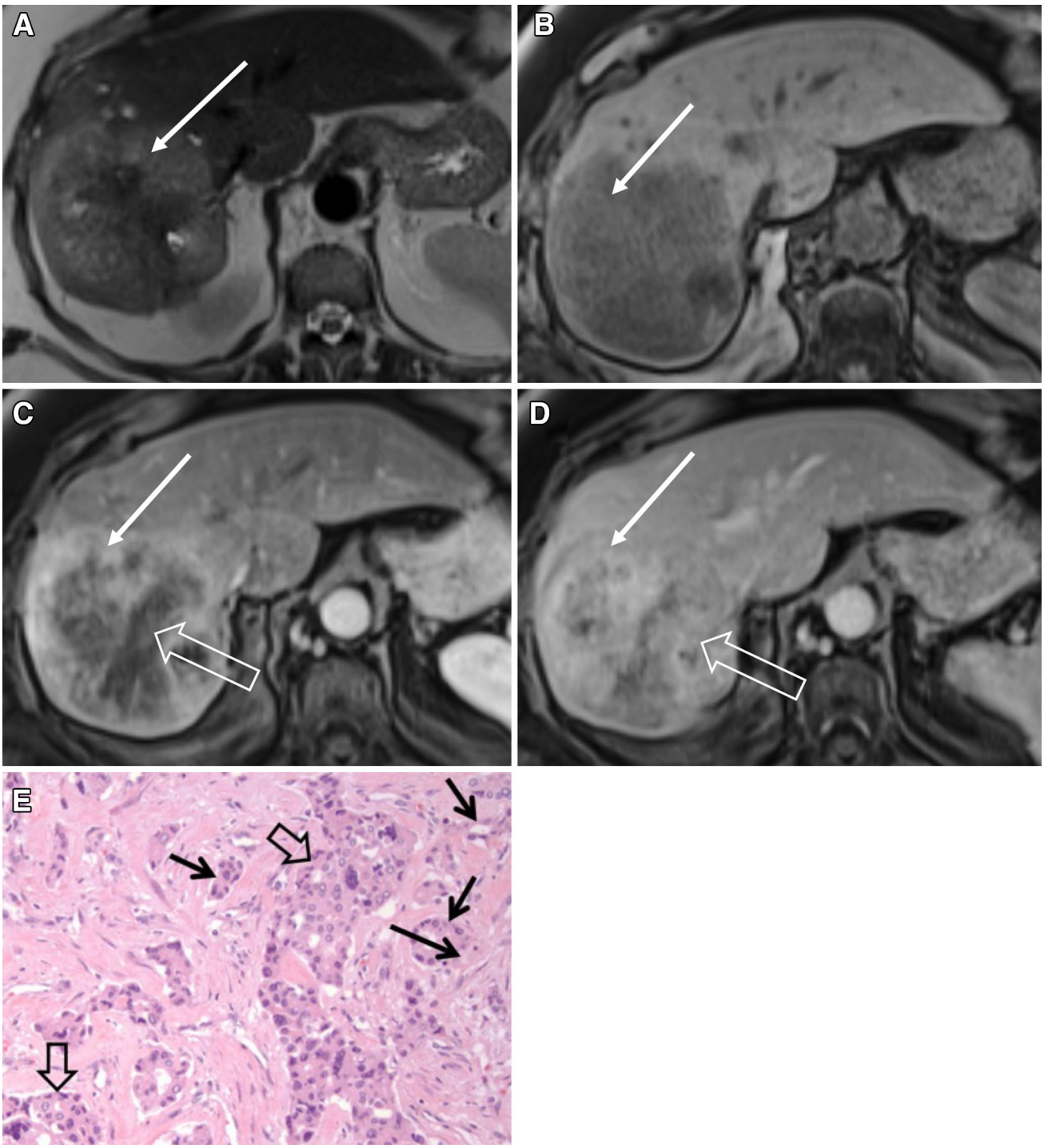

Fig. 16. Cholangiocellular carcinoma: **A** Axial T2-weighted image demonstrating a heterogeneous hyperintense lesion (*arrow*). **B** Precontrast axial T1-weighted image demonstrating a corresponding hypointense mass (*arrow*). **C** Arterial phase showing ring-like peripheral enhancement of the mass (*arrow*) but no enhancement of the central aspect of the lesion (*hollow arrow*). **D** Delayed post-contrast image demonstrating a progressive enhancement of the central aspect of the lesion (*hollow arrow*) but washout at the periphery (*arrow*). **E** Cholangiocellular carcinoma scattered irregularly shaped solid nests of cells with abundant eosinophilic cytoplasm consistent with hepatocellular differentiation (*hollow arrows*) admixed with small, angulated glands consistent with cholangiocarcinomatous differentiation (*solid arrows*) infiltrating within a desmoplastic stroma (H&E $\times$200).

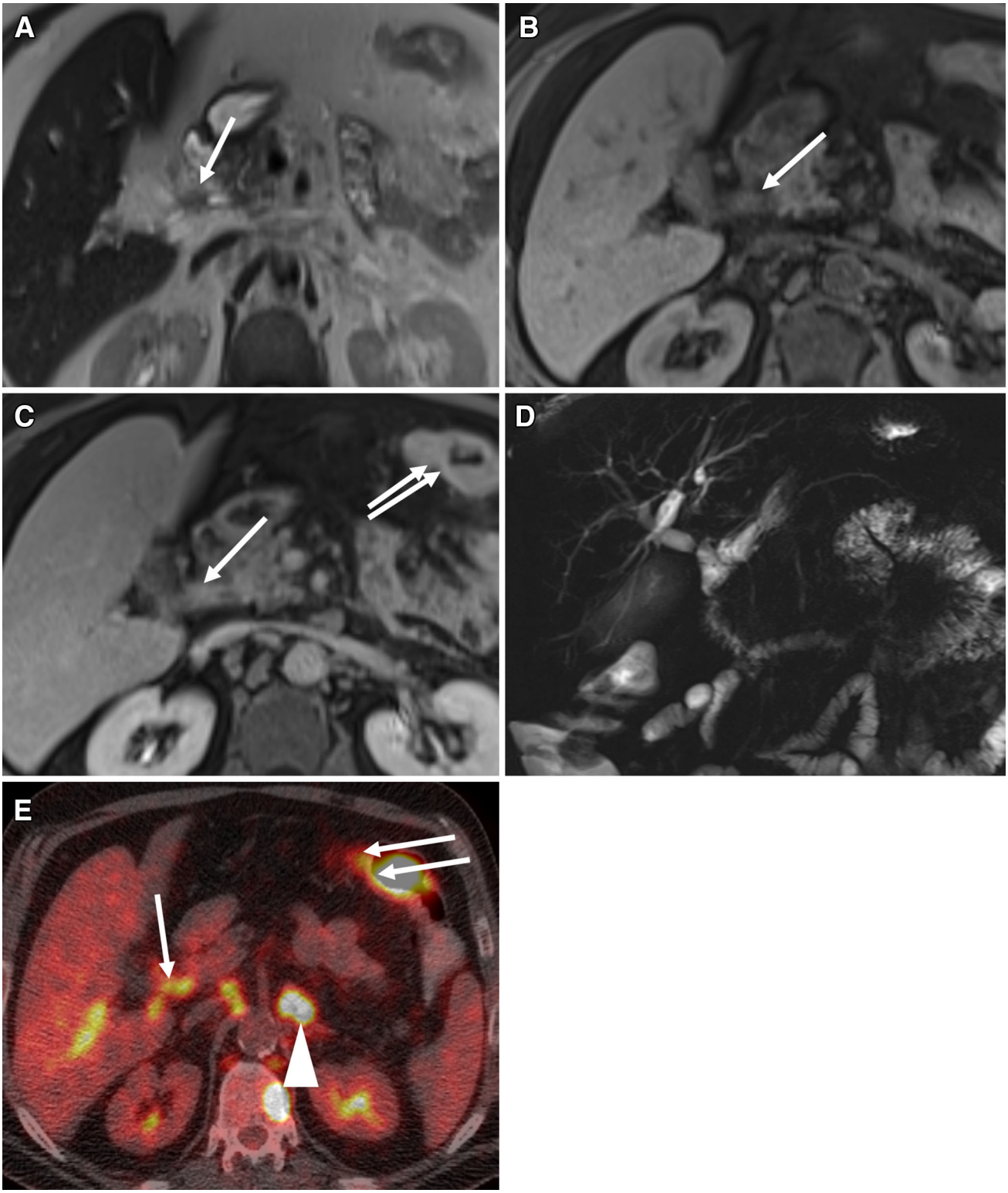

Fig. 17. Synchronous colon cancer metastasis to bile duct**:** **A** Axial T2-weighted image demonstrating a hypointense lesion involving the distal bile duct (*arrow*). **B** Axial precontrast T1-weighted image demonstrating the corresponding isointense signal (*arrow*). **C** Delayed post-contrast axial image demonstrating a progressive enhancing soft tissue (*arrow*), and there is also the thickening and enhancement of the splenic flexure of colon consistent with colon cancer (*double arrow*). **D** Coronal MRCP slab image showing stricture of the distal bile duct with upstream ductal dilatation. **E** PET scan showing metabolic activity in the distal bile duct and splenic flexure consistent with synchronous colon cancer (*double arrows*) with metastasis to bile duct (*arrow*). Metastatic node is also noted (*arrowhead*).

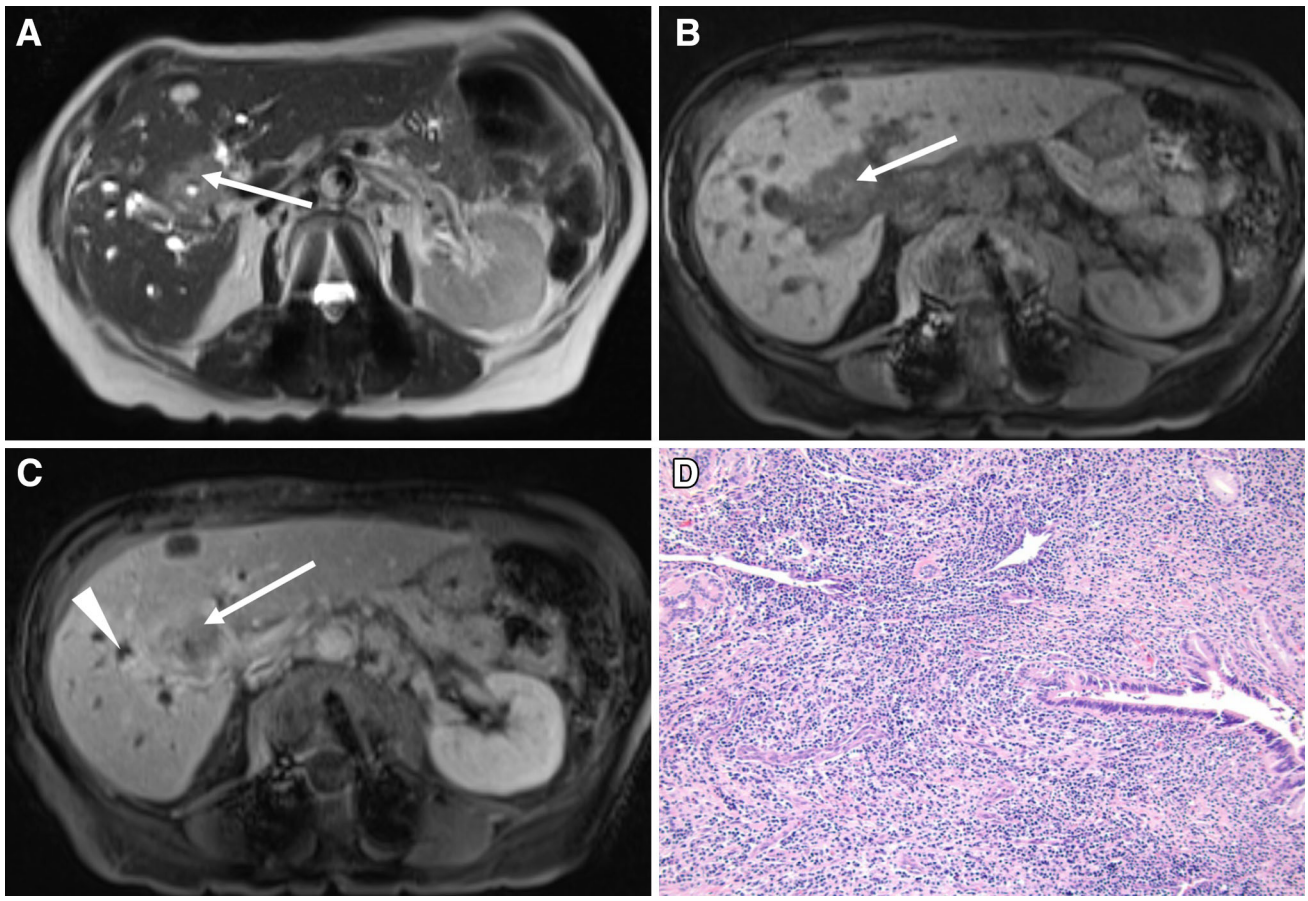

Fig. 18. Lymphoma: **A** Axial T2-weighted image demonstrating a hyperintense lesion surrounding the right hepatic duct (*arrow*). **B** Precontrast axial T1-weighted image demonstrating the corresponding low signal (*arrow*). **C** Delayed post-contrast axial image demonstrating a progressive enhancing soft tissue mass (*arrow*) with adjacent biliary ductal dilatation (*arrowhead*). **D** Large atypical lymphocytes showing diffuse growth pattern indicating diffuse large B cell lymphoma (H&E ×40).

Both large and small ducts are involved in 75% of adult cases whereas only small ducts or large ducts are involved in 15% and 10% of patients, respectively [71]. The lack of visualization of peripheral ducts due to a central ductal obliteration causes the pruned tree appearance.

MRCP is a noninvasive and cost-effective method to initially diagnose PSC and is comparable in both sensitivity (80%) and specificity (90%) to ERCP [78]. MRCP can depict more strictures, especially those of the peripheral intrahepatic ducts, and also provides better visualization of the bile ducts proximal to the obstructed area and not connected to the central ducts, which cannot be visualized due to nonfilling on ERCP. Therefore, ERCP should be reserved for patients who need biliary intervention, such as those who develop progressive jaundice and are found to have a dominant stricture, which raises the possibility of CCA [79]. Importantly, CCA may be present in 10–15% patients with stenotic lesions. A dominant stricture has been defined as stenosis with a diameter equal to or less than 1.5 mm in the common duct and 1.0 mm in hepatic duct [80]. There are no known biomarkers or surveillance-imaging protocols to screen for CCA in patients with PSC, but MRI or CT with contrast are useful in the detection of CCA complicating PSC. At MR imaging, findings suggesting the development of CCA in the setting of PSC include a focal mass, bile duct wall thickening, and progressive biliary obstruction at serial imaging [81].

Secondary sclerosing cholangitis (SSC)

SSC is a spectrum of chronic cholestatic diseases similar to PSC and occurs due to known pathological processes such as AIDS cholangiopathy, recurrent pyogenic cho-

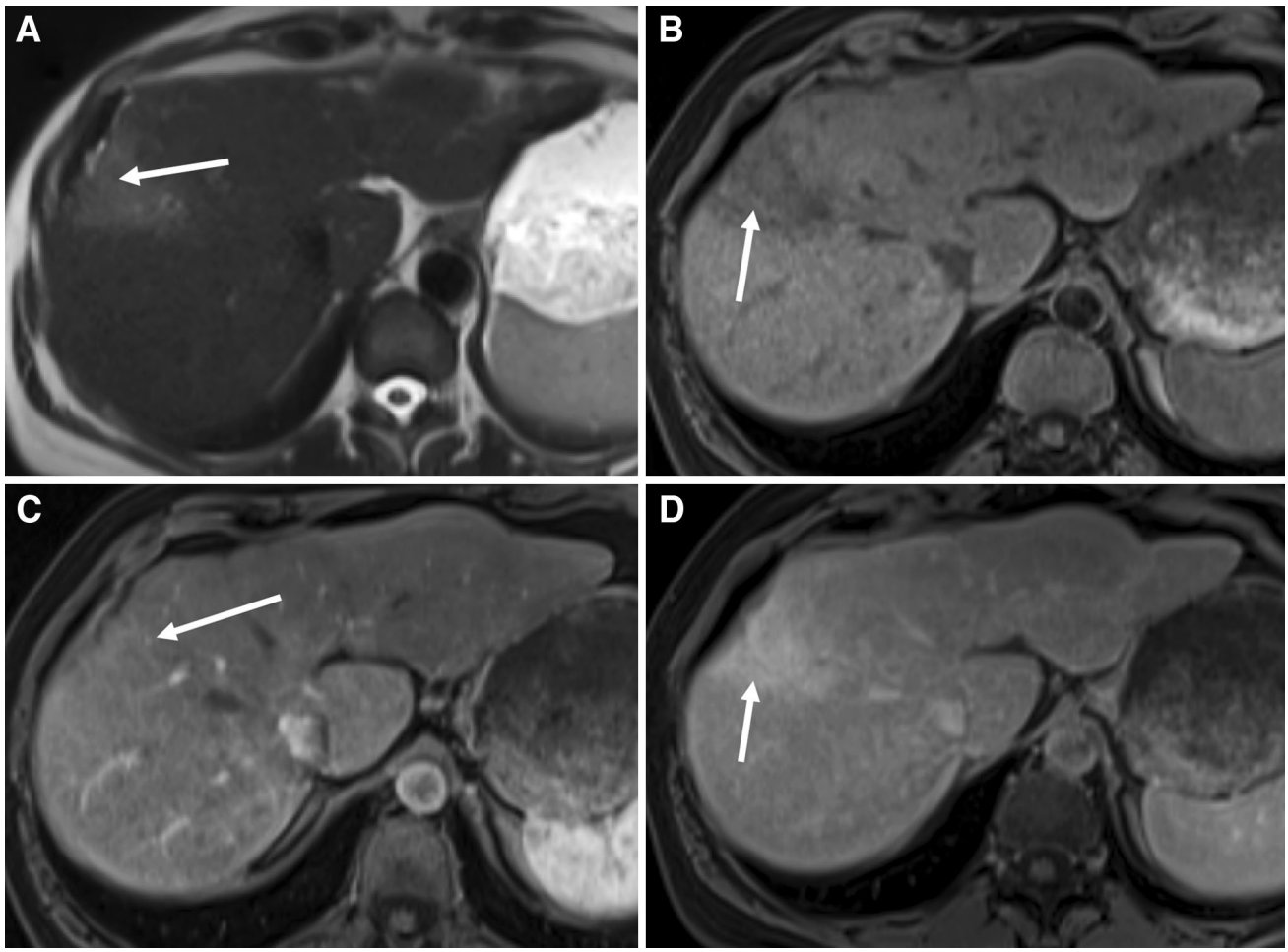

Fig. 19. Confluent fibrosis: **A** Axial T2-weighted image demonstrating a wedge-shaped hyperintense lesion in the anterior segment of right hepatic lobe and medial segment of left hepatic lobe (*arrow*). **B** Precontrast axial T1-weighted image demonstrating the corresponding low signal (*arrow*). **C** and **D** Arterial and delayed post-contrast axial images demonstrating progressive enhancement (*arrow*) with adjacent capsular retraction but no biliary ductal dilatation.

langitis, autoimmune pancreatitis, ischemic cholangiopathy, and trauma.

AIDS cholangiopathy

AIDS cholangiopathy is a biliary tract inflammation with stricture formation seen in severely immunocompromised AIDS patients with a CD4 count less than 100 mm^3 [82]. However, the incidence has decreased since the adoption of widespread use of highly active antiretroviral therapy (HAART). Several pathogens, including cytomegalovirus, cryptosporidium parvum, microsporidia, and microbacterium complex have been postulated to cause AIDS cholangiopathy. Patients usually present with epigastric and right upper quadrant pain due to papillary stenosis and biliary mucosal inflammation with edema. The large intrahepatic ducts are most commonly involved [83]. At MRCP, the hallmark of AIDS cholangiopathy is the variable association of extrahepatic biliary abnormalities such as papillary stenosis and long extrahepatic bile duct strictures with an intrahepatic pattern resembling PSC [84]. Papillary stenosis, either alone or in combination with intrahepatic irregularities, i.e., beaded appearance (Fig. 23), is present in 75% of cases [84], and dilated common duct tapers smoothly in the terminal portion.

Four patterns of AIDS cholangiopathy are noted on either ERCP or MRCP: (1) papillary stenosis, (2) intrahepatic sclerosing cholangitis, (3) intrahepatic biliary strictures associated with papillary stenosis, and (4) long

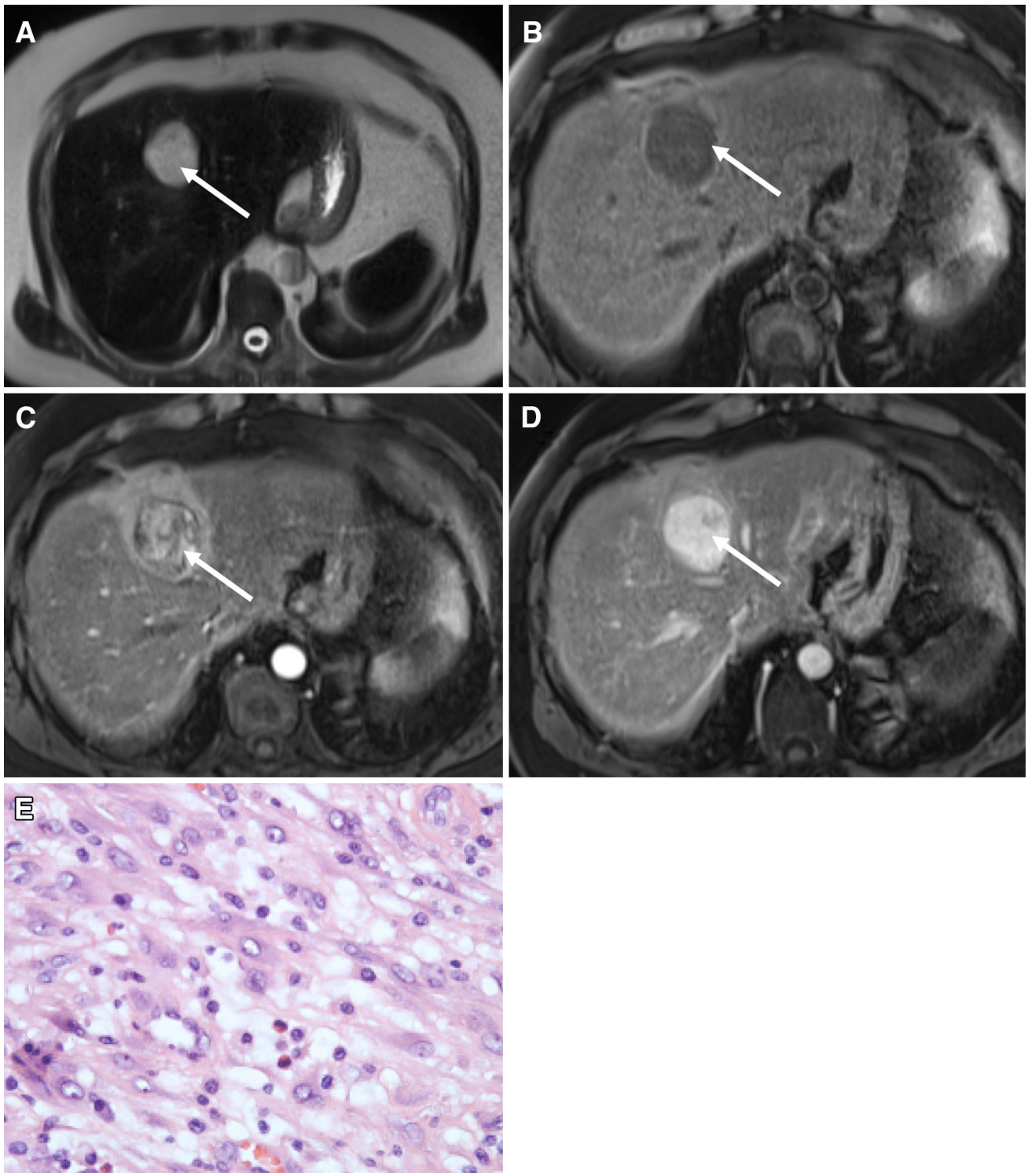

Fig. 20. Inflammatory myofibroblastic tumor**: A** Axial T2-weighted image demonstrating a hyperintense lesion involving segment 4A of left hepatic lobe (*arrow*). **B** Precontrast axial T1-weighted image demonstrating the corresponding low signal (*arrow*). **C** and **D** Arterial and delayed post-contrast axial images demonstrating a progressive enhancing soft tissue mass (*arrow*). **E** Inflammatory myofibroblastic tumor, streaming fusiform spindle cells with elongated nuclei, pale chromatin, and eosinophilic cytoplasm representing the myofibroblastic component with a smattering of inflammatory cells including lymphocytes, plasma cells, and eosinophils scattered throughout (H&E $\times$200).

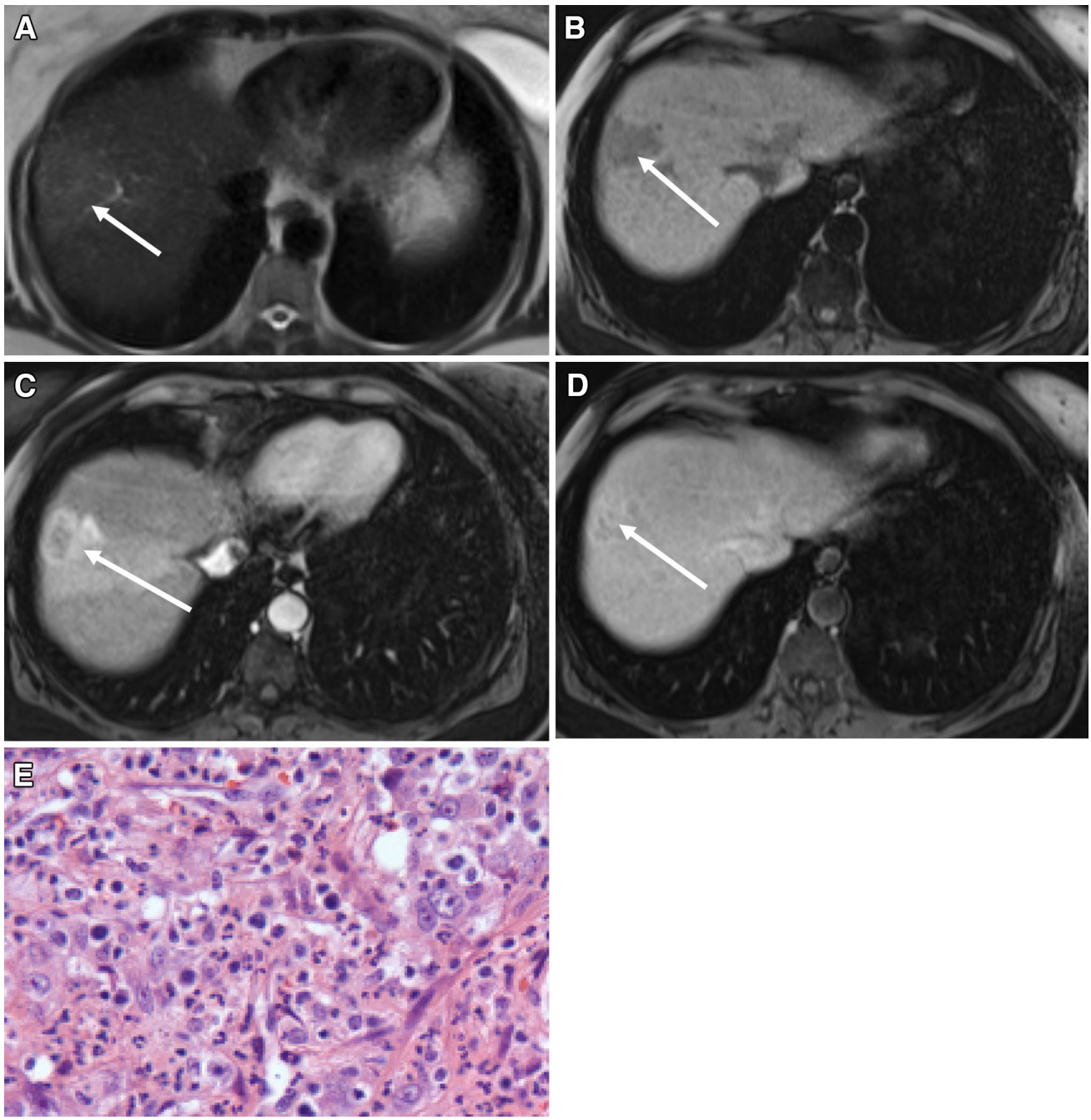

Fig. 21. Lymphoepithelioma-like carcinoma: **A** Axial T2-weighted image demonstrating a hyperintense lesion in the right hepatic duct segment 8 (*arrow*). **B** Precontrast axial T1-weighted image demonstrating the corresponding low signal (*arrow*). **C** and **D** Arterial and delayed post-contrast axial images demonstrating a progressive enhancing mass (*arrow*). **E** Lymphoepithelioma-like carcinoma, nodules of epithelioid cells with high nuclear-to-cytoplasmic ratio, large pleomorphic nuclei, pale chromatin, prominent nucleoli, and a small amount of pale eosinophilic cytoplasm set within a lymphocyte-rich stroma. The tumor nests themselves are also infiltrated by lymphocytes (H&E ×200).

extrahepatic biliary strictures with or without intrahepatic involvement [85, 86]. AIDS cholangiopathy can be accurately diagnosed with MRCP, so ERCP is reserved for when an interventional procedure, such as a sphincterotomy, stent placement for obstruction, or a biopsy to rule out malignancy, is required.

Recurrent pyogenic cholangitis (RPC)

RPC, also known as oriental cholangitis, is characterized by recurrent attacks of pyogenic cholangitis in the setting of obstruction by pigmented stones or biliary strictures. Clinically, the patient presents with repeated attacks of

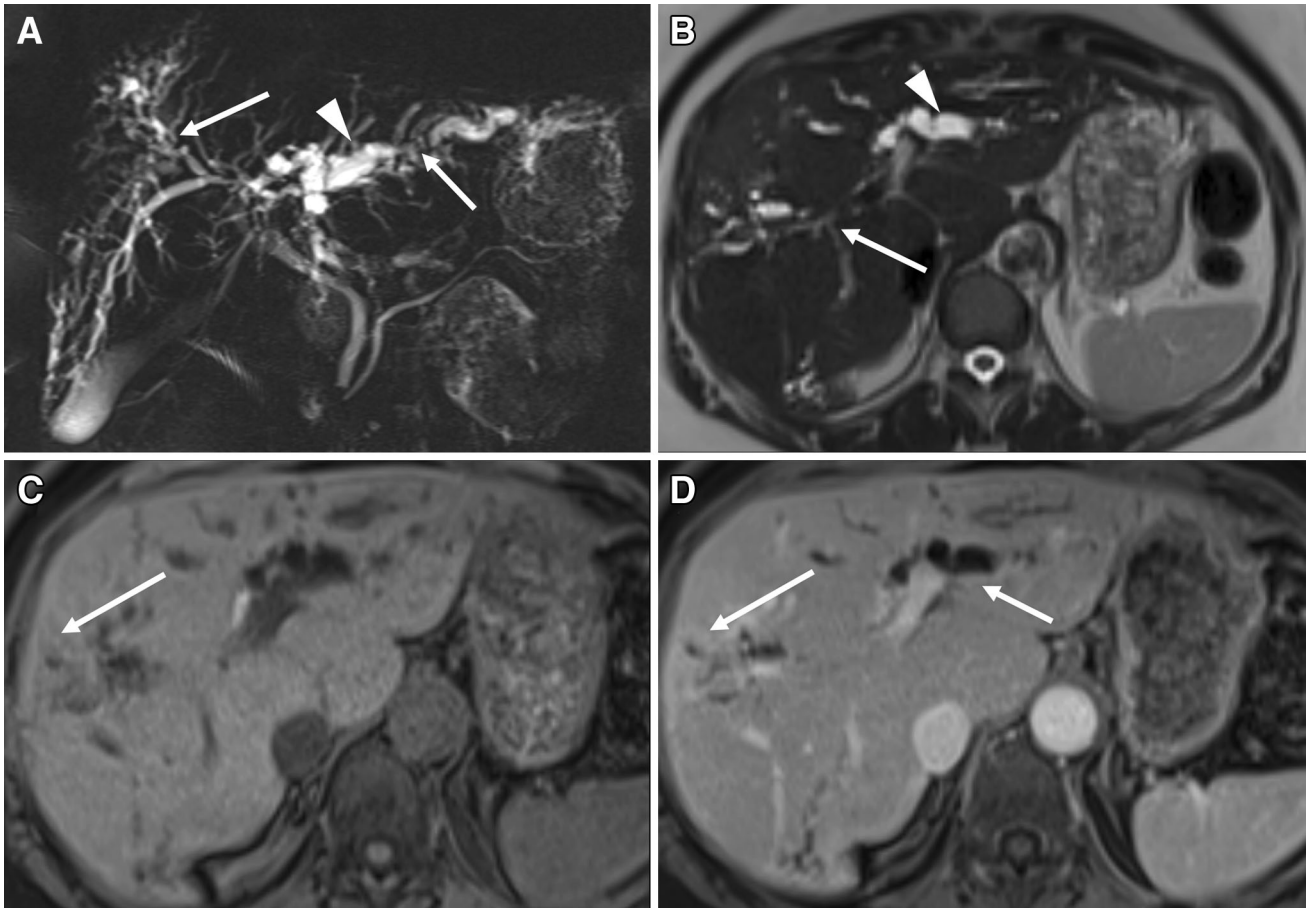

Fig. 22. Primary sclerosing cholangitis: **A** Coronal MRCP slab **B** axial T2WI demonstrating segmental strictures (*arrow*) and dilatation (*arrowhead*) of bile ducts giving beaded appearance. **C** Precontrast axial T1-weighted image demonstrating the corresponding thickening of the bile ducts (*arrow*). **D** Axial delayed phase post-contrast image demonstrating progressive periductal enhancement consistent with fibrosis (*arrow*).

fever, abdominal pain, and jaundice. Malnutrition, low socioeconomic status, and parasitic involvement by ascariasis and clonorchiasis are the main factors that cause bacterial colonization of recurrent inflammation and stone formation. Repeated attacks of inflammation result in scarring and fibrosis, resulting in biliary strictures and dilatation [87]. At MR imaging, findings include biliary strictures, ductal wall thickening secondary to fibrosis which show progressive delayed enhancement, and intraductal pigment stones which are hyperintense on T1WI (Fig. 24) [88]. The lateral segment of the left hepatic lobe and the posterior segment of the right hepatic lobe and extrahepatic ducts are most commonly involved in RPC [89]. The ductal wall thickening and progressive delayed enhancement can mimic CCA. On the other hand, RPC has a 2–6% increased risk of CCA. The management of RPC depends on the extent of the disease; surgical resection is considered if disease is confined to a single segment or lobe whereas percutaneous drainage procedures are recommended for unresectable disease.

Autoimmune pancreatitis (AIP), IgG4 cholangiopathy

Secondary sclerosing cholangitis (SSC) can be associated with autoimmune sclerosing pancreatitis. This reveals high levels of IgG4 in blood and histological specimens which is specific for autoimmune pancreatitis, and is more common in males with an average age of 55 years. AIP can present clinically as a primary pancreatic disorder or a systemic autoimmune (extra pancreatic) disorder with extensive involvement of the bile ducts, gall bladder, kidneys, salivary glands, thyroid gland, and retroperitoneum, which can be synchronous or metachronous to the pancreas, and demonstrates elevated levels

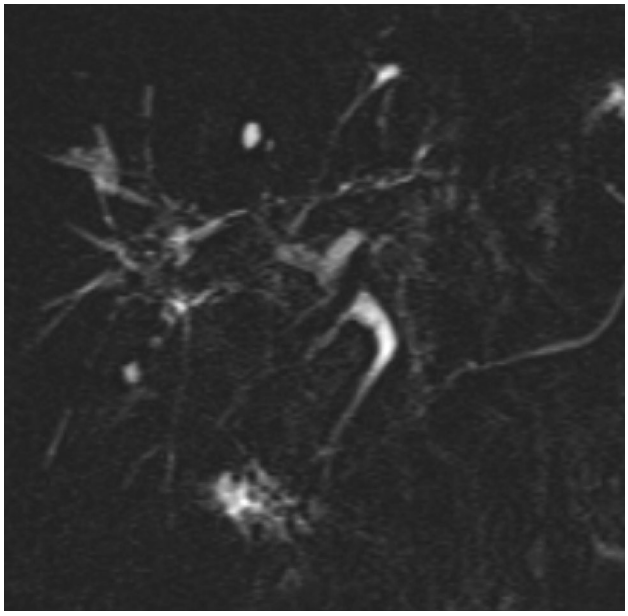

Fig. 23. AIDS cholangiopathy: A 46-year-old male with AIDS. Coronal MRCP slab showing stricturing and dilatation of the intrahepatic and extrahepatic biliary ducts mimicking primary sclerosing cholangitis.

of IgG4 [90, 91]. Histologically, AIP is characterized by diffuse lymphocytic infiltration, interstitial fibrosis, acinar atrophy, obliterative phlebitis within the pancreas, and IgG4 plasma cells in bile duct specimens [92]. Clinical symptoms are usually related to acute or chronic pancreatitis, biliary or pancreatic strictures, and obstructive jaundice (observed in 40% of patients in one series) [93]. Imaging features of AIP include diffuse or focal enlargement of the pancreas with a peripheral halo and focal or diffuse stricture of the pancreatic duct [94]. Biliary strictures are classified into four types: (1) diffuse stricture of the intra- and extrahepatic bile ducts, (2) distal bile duct stricture, (3) hilar and distal bile duct stricture, and (4) isolated hilar stricture [95]. MR imaging demonstrates a thick symmetric circumferential ring of enhancing tissue surrounding the stricture (Fig. 25) and a narrowing of the intrahepatic ducts and bile duct strictures with upstream dilatation, which mimics CCA. High levels of IgG4 and significant improvement after steroid administration differentiates between CCA and sclerosing cholangitis.

Ischemic cholangiopathy

Ischemic cholangiopathy is defined as focal or generalized damage to the bile ducts due to impaired blood supply either at the level of the main hepatic duct branches or at the peribiliary capillary plexus and has an incidence of 2–10% in liver transplant recipients [82]. Ischemic bile duct injury may cause bile duct necrosis, bile leakage, biloma, bile duct fibrosis, or stenosis. The predominant site of involvement is the middle third of the common bile duct, followed by the hepatic duct confluence and intrahepatic duct involvement [96]. MRCP findings resemble those of PSC with multiple nonanatomic strictures and biliary tree dilatation. Potentially obstructing biliary casts may be present and are composed of bilirubin, components of bile acids, cholangiocyte fragments and bacteria.

Other conditions contributing to vascular injury to bile ducts include hepatic artery infusion (chemo therapeutic agents), hereditary hemorrhagic telangiectasia, radiotherapy to the liver area, polyarteritis nodosa, trauma, and post-cholecystectomy strictures [97].

Chemotherapy-induced biliary sclerosis

Hepatic artery infusion of fluropyrimidines (floxuridine and florouracil) has been widely used for the treatment of colorectal metastases to the liver and had been implicated as a cause of secondary biliary sclerosing cholangitis. The incidence ranges from 8% to 26% [98]. Drug-induced intravascular thrombosis and toxic vasculitis have been suggested as possible mechanisms which lead to ischemic insult and stricture formation [98]. To minimize the risk of chemotherapy-induced sclerosing cholangitis, several approaches have been suggested, including dose reduction and addition of steroids to the regimen. Once chemotherapy-induced biliary sclerosis has developed, therapeutic approaches include endoscopic, surgical, or percutaneous drainage of the biliary system. At MR imaging, the most common findings are strictures at the bifurcation of common hepatic duct with sparing of the distal bile duct (Fig. 26).

Post-traumatic sclerosing cholangitis

Post-traumatic sclerosing cholangitis is probably caused by ischemia of the intrahepatic bile ducts normally supplied via the peribiliary capillary plexus due to arterial hypotension and marked cholestasis following severe trauma. It is assumed that hypoperfusion, possibly aggravated by vasopressors, causes ischemic change to the intrahepatic bile ductal epithelium leading to scarring of the ducts and subsequent cholestasis. Post-traumatic sclerosing cholangitis mainly involves the intrahepatic ducts as a consequence to a limited blood supply by peribiliary complexes, whereas the extrahepatic biliary

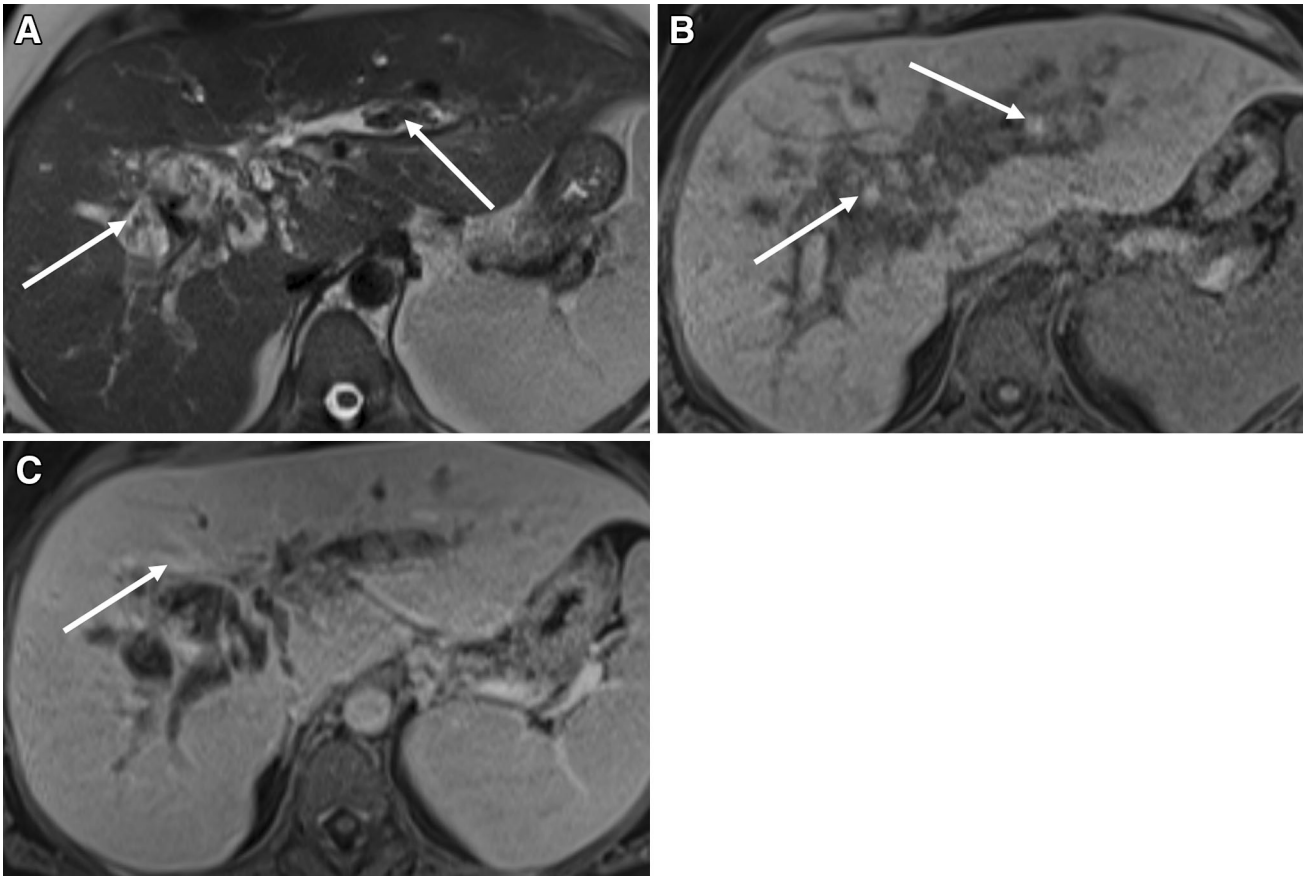

Fig. 24. Recurrent pyogenic cholangitis: **A** Axial T2-weighted image demonstrating segmental biliary dilatation and strictures involving the lateral segment of left hepatic lobe and posterior segment of right hepatic lobe with associated T2 hypointense filling defects consistent with hepatolithiasis (*arrows*). **B** Precontrast axial T1-weighted image demonstrating the corresponding T1 hyperintense filling defects consistent with intraductal pigment stones (*arrows*). **C** Delayed post-contrast image demonstrating the thickening of the ductal wall and progressive enhancement due to fibrosis (*arrow*).

system has a more robust supply from two arteries running parallel to the common bile duct fed by the gastroduodenal, retroduodenal, and right and left hepatic arteries [99]. At MR imaging, findings are similar to PSC with strictures and dilatation of the intrahepatic ducts (Fig. 27).

Iatrogenic biliary strictures

The most common cause of iatrogenic bile duct strictures is prior hepatobiliary surgery. In particular, a cholecystectomy accounts for 80% of cases [100, 101]. The incidence of post-cholecystectomy stricture is 0.2–0.7% for an open cholecystectomy but up to 1.2% in laparoscopic cholecystectomies [102, 103]. Post-cholecystectomy strictures often involve the extrahepatic duct, and the most common site is at the junction of the cystic duct with the common hepatic duct and the confluence of the right and left hepatic ducts [104]. Vascular injuries are reported along with bile duct injury in some cases, especially to the hepatic artery [105, 106].

Only 20% of bile duct injuries are noted intraoperatively, and 25% of patients with an unrecognized injury present within 1 week and 50% within 1 month with various degrees of biliary obstruction [107]. In long-standing obstruction, strictures can mimic CCA. At MR imaging, the narrowed segment commonly demonstrates a thin nonenhancing wall with smooth margins. However, in long-standing biliary obstruction, ductal reaction with accompanying inflammation and fibroplasia shows progressive delayed enhancement on contrast-enhanced MRI and mimics CCA (Fig. 28). It is important to recognize biliary obstruction early on because relieving the bile duct obstruction may lead to reversal of the parenchymal and portal changes. However, extensive periductal and periportal fibrotic changes and secondary biliary cirrhosis are irreversible.

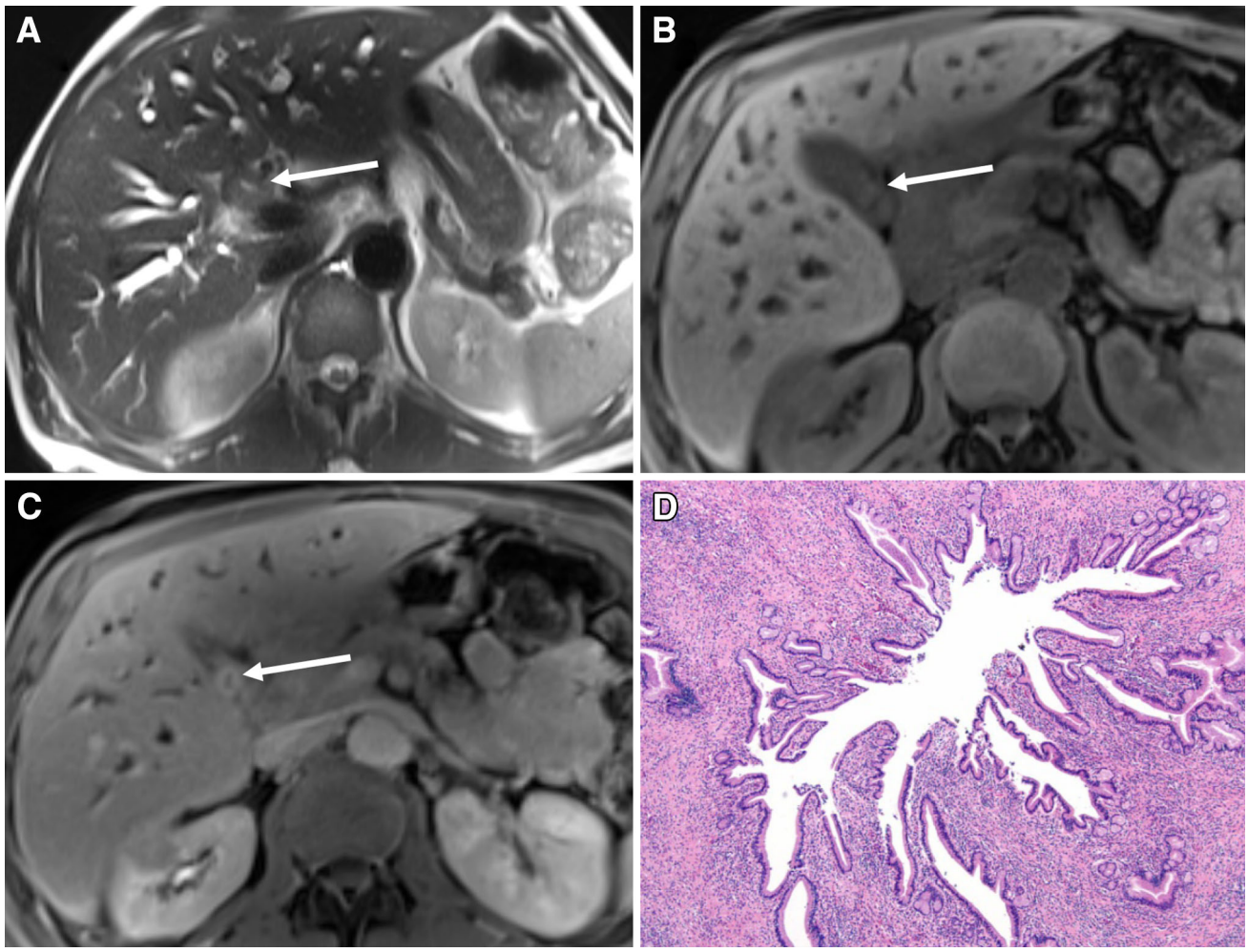

Fig. 25. Autoimmune sclerosing (IgG4) cholangitis: **A** Axial T2-weighted image showing a slightly hyperintense signal and **B** Axial precontrast T1-weighted image demonstrating a hypointense circumferential thickening of the bile duct at the confluence. **C** Axial delayed post-contrast image showing a symmetric circumferential ring of enhancing tissue surrounding the stricture (*arrow*). **D** Autoimmune sclerosing (IgG4) cholangitis-mixed inflammatory infiltrate is composed of lymphocytes, plasma cells, and eosinophils (H&E ×40).

Ampullary/periampullary carcinoma

Ampullary/periampullary carcinomas are a group of tumors consisting of carcinomas of the ampulla of Vater, periampullary duodenum, and distal common bile duct tumors. These tumors have a similar presentation to pancreatic head carcinomas and cause obstruction of the common bile duct and pancreatic duct. Periampullary carcinomas cause obstruction even if they are only a few millimeters in size and not apparent on imaging; as such, isolated dilatation of the biliary and pancreatic ducts can be observed early in the course of the disease. As a result, these cancers become clinically symptomatic early and consequently have a better prognosis, as compared to pancreatic carcinomas, with a 5-year survival rate of up to 85% [108]. Marked and abrupt dilatation of the distal bile duct or pancreatic duct is suggestive of ampullary carcinoma in the absence of stone disease or pancreatitis [109]. Ampullary carcinoma manifests as a small mass/nodule, periductal thickening, or bulging of duodenal papilla whereas distal duct carcinoma manifests as a luminal obliteration and wall thickening or polyploid mass. In patients with periampullary carcinoma of bile duct origin, the pancreatic duct is often normal—mimicking distal bile duct CCA until the tumor invades the

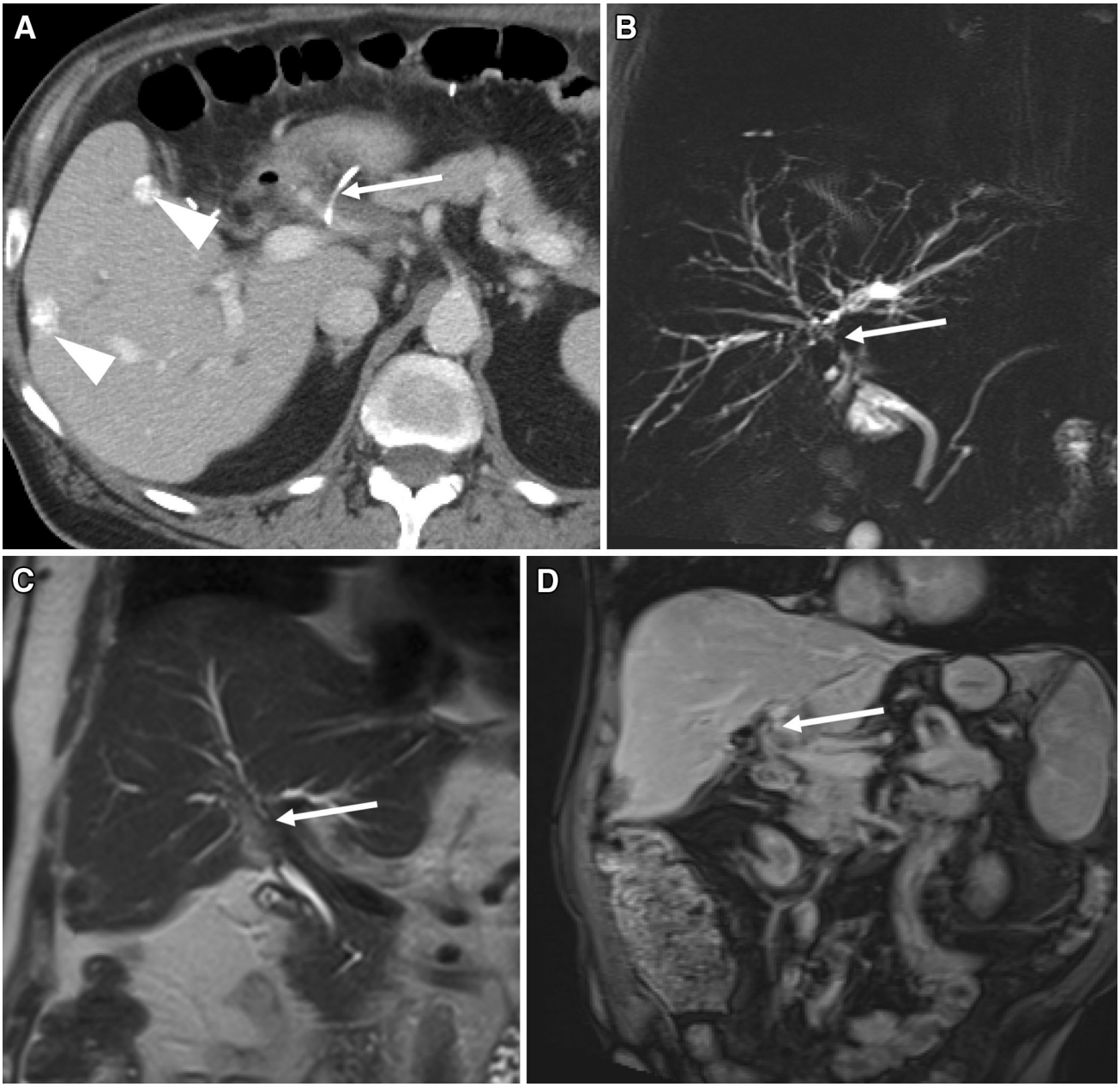

Fig. 26. Chemotherapy-induced biliary sclerosis**: A** Axial post-contrast CT scan image demonstrating hepatic artery infusion pump catheter (*arrow*) and calcified hepatic metastatic lesions (*arrowheads*). **B** Coronal MRCP slab image demonstrating stricture at the confluence (*arrow*) causing intrahepatic ductal dilatation. **C** Coronal T2-weighted image showing long stricture at the confluence with associated hyperintensity due to edema (*arrow*). **D** Delayed post-contrast coronal T1-weighted image showing progressive delayed enhancement consistent with fibrosis (*arrow*).

ampullary portion or directly invades the pancreatic duct through the pancreatic parenchyma [109]. At MR imaging, these tumors are iso- to hypointense on pre-contrast T1WI and T2WI and are poorly or moderately enhancing following contrast administration as compared to pancreatic parenchyma [110]. MRCP is a very useful diagnostic tool to visualize biliary and pancreatic duct dilatation and the level of obstruction (Fig. 29).

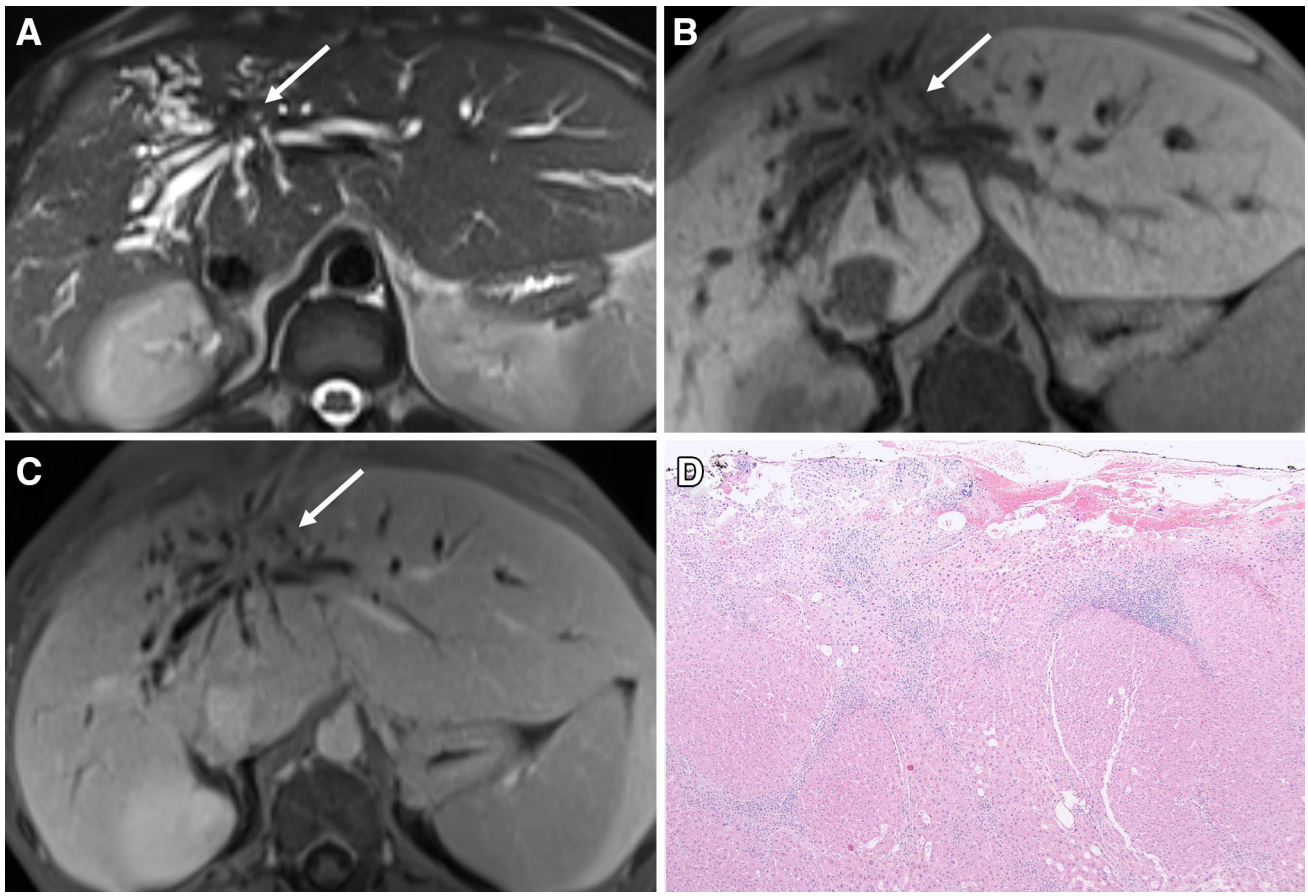

Fig. 27. Post-traumatic stricture: A 29-year-old male with remote history of gunshot wound to the abdomen. **A** Axial T2-weighted image demonstrating a mildly hyperintense mass at the confluence (*arrow*) predominantly in segments 8 and 4A, causing intrahepatic biliary ductal dilatation, right greater than left. **B** Precontrast axial T1-weighted image demonstrating a corresponding hypointense mass (*arrow*). **C** Delayed post-contrast axial image demonstrating progressive enhancement (*arrow*) and capsular retraction mimicking cholangiocarcinoma but with a fibrous scar. **D** Liver parenchyma with bile stasis and fibroadipose tissue (H&E ×40).

Periampullary carcinomas share similar anatomic locations, clinical features, and therapeutic approaches, but their long-term outcome varies. MRCP and MRI are helpful in determining the origins of periampullary carcinomas.

Mirizzi syndrome

First described by Mirizzi in 1948, Mirrizi syndrome is characterized by the presence of a common hepatic duct obstruction caused by an extrinsic compression of impacted stone in the gallbladder neck or cystic duct. It is present in 0.35% of cholecystectomies [111]. Low insertion of the cystic duct into the common hepatic duct is a predisposing factor. MRI and MRCP are most sensitive in the diagnosis of Mirizzi syndrome with high sensitivity and specificity. Typical findings are narrowing of the common hepatic duct by extrinsic compression due to stones in the cystic duct or gall bladder neck and dilatation of the intrahepatic ducts and common hepatic duct with a normal common bile duct. Subsequent inflammation around the bile duct leads to stricture

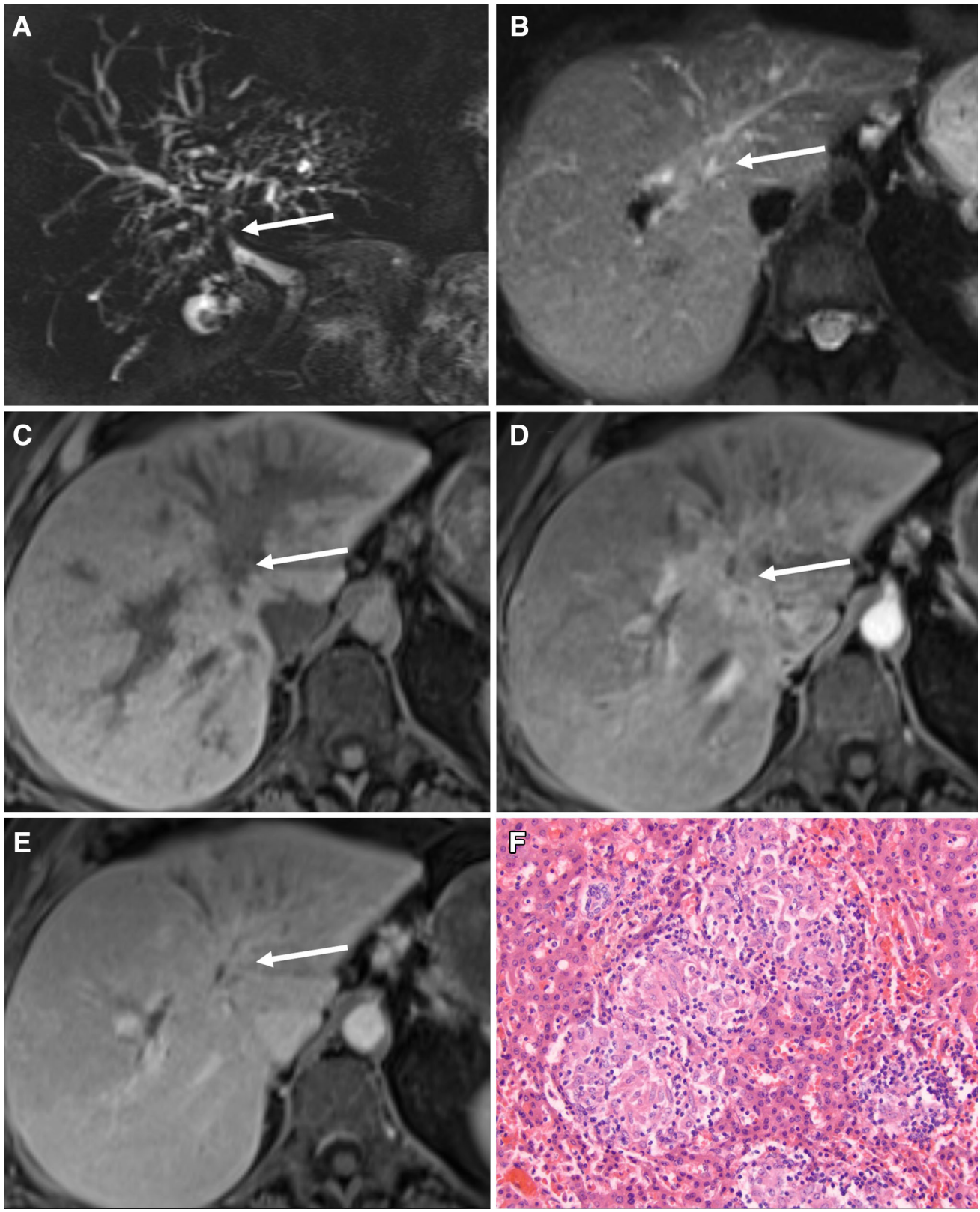
A
B
C
D
E
F

◀ **Fig. 28.** Iatrogenic post-cholecystectomy biliary stricture: **A** Coronal MRCP slab demonstrating stricture at the confluence (*arrow*) causing intrahepatic ductal dilatation, left greater than right. **B** Axial T2 fat sat (SPAIR) image demonstrating a hyperintense signal in the hilar region (*arrow*) due to edema. **C** Precontrast axial T1-weighted image demonstrating the corresponding low signal (*arrow*). **D** and **E** Arterial and delayed post-contrast images demonstrating the thickening of the strictured bile ducts and peribiliary progressive enhancement mimicking cholangiocarcinoma (*arrows*). **F** Extensive ulceration, fibrosis, and granulation tissue formation of the bile duct, no neoplastic cells (H&E ×100).

formation, which mimics periductal infiltrating CCA (Fig. 30) [111, 112].

Recent advances

Role of hepatobiliary specific agents

Gadoxetate disodium (Gd-EOB-DTPA) is a hepatobiliary specific agent that is 50% excreted by the liver and 50% by the kidneys in patients with normal hepatic and renal function and is typically excreted into the biliary system within 7–10 min of administration, with serial

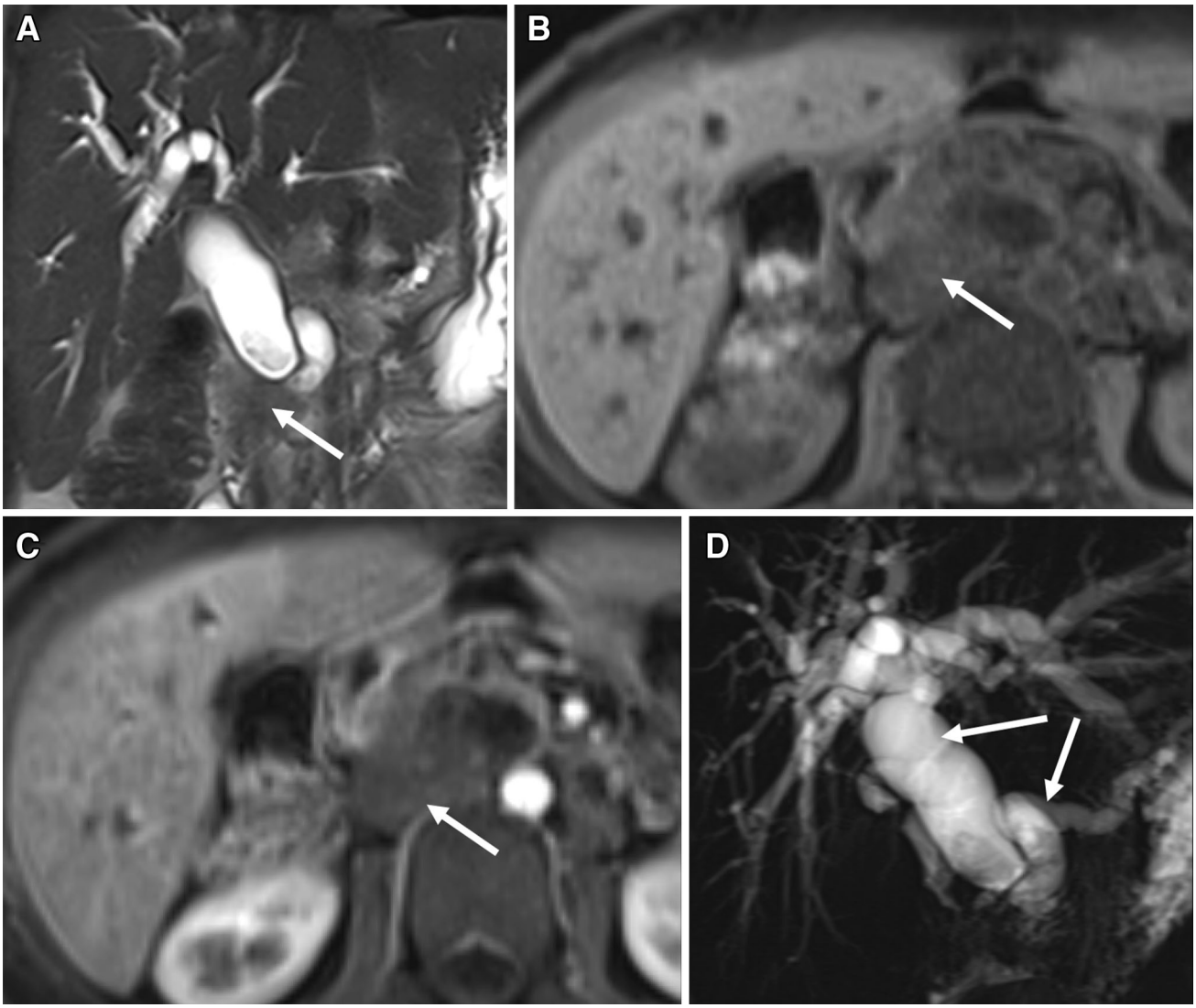

Fig. 29. Ampullary carcinoma**: A** Coronal T2-weighted image demonstrating a hypointense lesion in the ampullary region (*arrow*). **B** Precontrast axial T1-weighted image demonstrating the corresponding low signal (*arrow*). **C** Delayed post-contrast image demonstrating a mild progressive enhancing soft tissue in the ampullary region (*arrow*). **D** Coronal MRCP slab demonstrating narrowing in the ampullary region with common bile duct and pancreatic duct dilatation (double duct sign) (*arrows*).

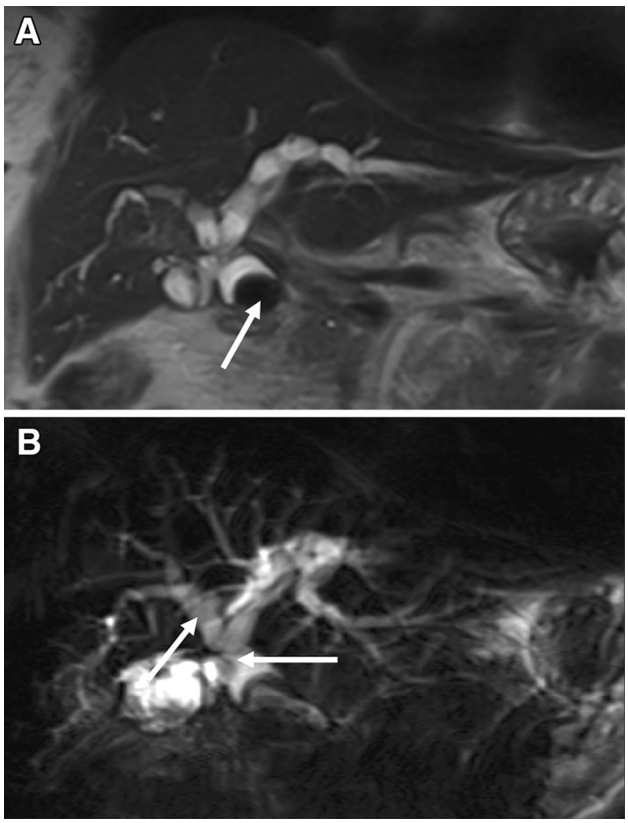

Fig. 30. Mirizzi syndrome: **A** Coronal T2-weighted MR image demonstrating an impacted gallstone in the cystic duct with resultant obstruction of the common hepatic duct (*arrow*). **B** Coronal MRCP slab demonstrating upstream dilatation of the common hepatic duct and intrahepatic ducts (*arrows*).

imaging obtained through 20-min (hepatobiliary phase) post injection. The optimum excretion of gadoxetate disodium into the biliary system depends on properly functioning hepatocytes because conditions such as acute or chronic hepatitis and bile duct obstruction may not take up or excrete contrast into the biliary system reliably. Gd-EOB-DTPA has approximately 50% higher intrahepatocyte T1 relaxivity because of reversible interactions with proteins, which is of clinical importance due to the substantial amount of Gd-EOB-DTPA located within the hepatocytes during the hepatobiliary phase [113].

Fig. 31. Cholangiocarcinoma with Gadoxetate disodium (Gd-EOB-DTPA) and DWI: **A** Axial T2-weighted MR demonstrating a hyperintense mass (*arrow*) in segment 5 of the liver. **B** Axial precontrast T1W image demonstrating a corresponding hypointense mass (*arrow*). **C** Arterial phase postcontrast axial MR image demonstrating a heterogeneous enhancement along the periphery of the lesion (*arrow*) relative to adjacent normal liver. **D** Axial 3-min delayed postcontrast MR image demonstrating progressive enhancement (*arrow*). **E** Axial 20-min delayed hepatobiliary phase demonstrating the enhancement of the liver due to hepatocyte uptake (*black arrow*), whereas cholangiocarcinoma appears hypointense due to the lack of functioning hepatocytes (*white arrow*). **F** DWI at $b = 1000$ s/mm^2 showing an intrahepatic cholangiocarcinoma with high signal intensity. ▶

At MR imaging, intrahepatic mass-forming CCAs are hypointense on precontrast T1WI and hyperintense on T2W imaging, but are variable depending on the amount of fibrosis, necrosis, and mucin within the tumor. Irregular peripheral rim enhancement during the arterial phase may be seen with Gd-EOB-DTPA because of its fibrous stroma, but delayed washout is typical for CCA when extracellular contrast agents are used. However, after Gd-EOB-DTPA injection, the surrounding liver enhances more because of the hepatocyte uptake, causing a hypointense appearance of the CCA during the hepatobiliary phase against the liver background due to the absence of functioning hepatocytes and allows better demarcation of the lesion (Fig. 31**A**–**E**) [1].

Role of diffusion-weighted MRI

CCAs have high signal intensity on high *b*-value ($b = 1000$ s/mm^2) images (Fig. 29**F**) and usually low ADC values due to high cellular content. It is difficult to distinguish between ICC, HCC, and metastases based on high signal intensity of the lesion on high *b*-value diffusion-weighted MRI (DW-MRI) and low ADC values. Thus, diffusion-weighted imaging (DWI) should be used along with conventional MRI sequences, such as dynamic enhanaced MRI, to differentiate CCA from other hepatic malignancies (Fig. 31**F**) [114]. High *b*-value DW-MRI may also be useful in differentiating malignant obstruction (e.g., bile duct cancer and pancreatic cancer)

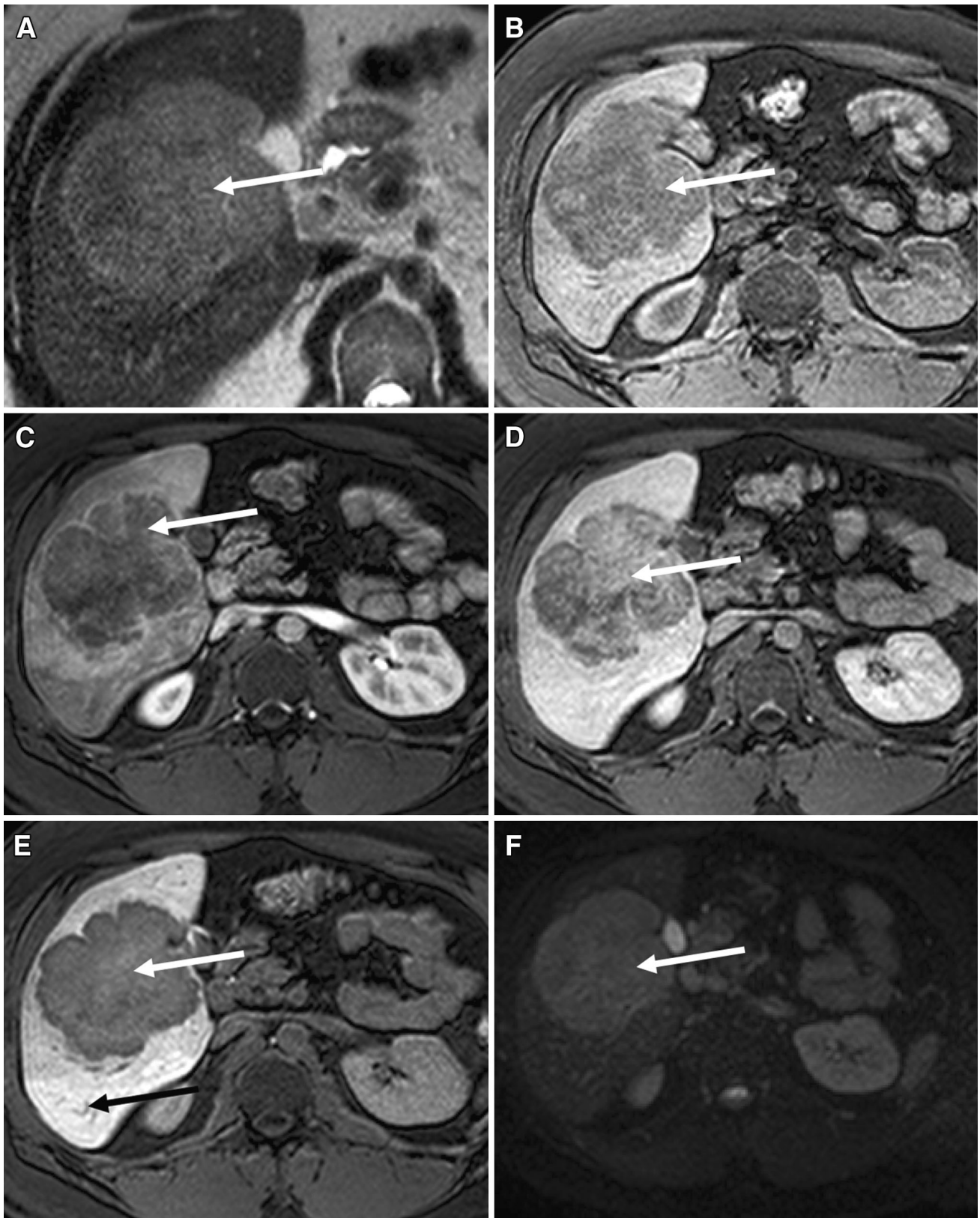
A
B
C
D
E
F

from benign obstruction (e.g. choledocholithiasis or benign stricture).

Conclusion

A variety of conditions resemble primary intra- or extrahepatic biliary conditions on imaging. Accurate characterization is required in order to narrow the differential diagnosis, as management and clinical outcomes vary. This can be achieved with contrast-enhanced MRI along with MRCP, a protocol that has become widely accepted by clinicians as the gold standard in the characterization of biliary conditions. ERCP should be reserved for those patients who require intervention, such as a stent placement to relieve obstruction or a biopsy for histopathological diagnosis, which cannot be made by MRI and MRCP alone. Some lesions, such as PSC, require watchful surveillance, while others, such as IgG4 cholangiopathy and malignant strictures, require medical and surgical management, respectively.

Acknowledgment. No grant support or other financial support was received by any of the authors during the creation of this manuscript.

References

1. Peporte AR, Sommer WH, Nikolaou K, Reiser MF, Zech CJ (2013) Imaging features of intrahepatic cholangiocarcinoma in Gd-EOB-DTPA-enhanced MRI. Eur J Radiol 82(3):e101–e106. doi:10.1016/j.ejrad.2012.10.010
2. Olnes MJ, Erlich R (2004) A review and update on cholangiocarcinoma. Oncology 66(3):167–179. doi:10.1159/000077991
3. Lim JH (2003) Cholangiocarcinoma: morphologic classification according to growth pattern and imaging findings. Am J Roentgenol 181(3):819–827. doi:10.2214/ajr.181.3.1810819
4. Nakajima T, Kondo Y, Miyazaki M, Okui K (1988) A histopathologic study of 102 cases of intrahepatic cholangiocarcinoma: histologic classification and modes of spreading. Hum Pathol 19(10):1228–1234
5. Ahrendt SA, Nakeeb A, Pitt HA (2001) Cholangiocarcinoma. Clin Liver Dis 5(1):191–218
6. Khan SA, Thomas HC, Davidson BR, Taylor-Robinson SD (2005) Cholangiocarcinoma. Lancet 366(9493):1303–1314. doi:10.1016/S0140-6736(05)67530-7
7. Poultsides GA, Zhu AX, Choti MA, Pawlik TM (2010) Intrahepatic cholangiocarcinoma. Surg Clin North Am 90(4):817–837. doi:10.1016/j.suc.2010.04.011
8. Lazaridis KN, Gores GJ (2005) Cholangiocarcinoma. Gastroenterology 128(6):1655–1667
9. Ayuso JR, Pages M, Darnell A (2013) Imaging bile duct tumors: staging. Abdom Imaging 38(5):1071–1081. doi:10.1007/s00261-013-0021-9
10. Razumilava N, Gores GJ (2014) Cholangiocarcinoma. Lancet . doi:10.1016/S0140-6736(13)61903-0
11. Ishikawa K, Sasaki A, Haraguchi N, Yoshikawa Y, Mori M (2007) A case of an alpha-fetoprotein-producing intrahepatic cholangiocarcinoma suggests probable cancer stem cell origin. Oncologist 12(3):320–324. doi:10.1634/theoncologist.12-3-320
12. Chung YE, Kim MJ, Park YN, et al. (2009) Varying appearances of cholangiocarcinoma: radiologic-pathologic correlation. Radiographics 29(3):683–700. doi:10.1148/rg.293085729
13. Vilgrain V, Van Beers BE, Flejou JF, et al. (1997) Intrahepatic cholangiocarcinoma: MRI and pathologic correlation in 14 patients. J Comput Assist Tomogr 21(1):59–65
14. Murakami T, Nakamura H, Tsuda K, et al. (1995) Contrast-enhanced MR imaging of intrahepatic cholangiocarcinoma: pathologic correlation study. J Magn Reson Imaging 5(2):165–170
15. Ros PR, Buck JL, Goodman ZD, Ros AM, Olmsted WW (1988) Intrahepatic cholangiocarcinoma: radiologic-pathologic correlation. Radiology 167(3):689–693. doi:10.1148/radiology.167.3.2834769
16. Vanderveen KA, Hussain HK (2004) Magnetic resonance imaging of cholangiocarcinoma. Cancer Imaging 4(2):104–115. doi:10.1102/1470-7330.2004.0018
17. Park HS, Lee JM, Kim SH, et al. (2006) CT differentiation of cholangiocarcinoma from periductal fibrosis in patients with hepatolithiasis. Am J Roentgenol 187(2):445–453. doi:10.2214/AJR.05.0247
18. Lee JW, Han JK, Kim TK, et al. (2000) CT features of intraductal intrahepatic cholangiocarcinoma. Am J Roentgenol 175(3):721–725. doi:10.2214/ajr.175.3.1750721
19. Barton JG, Barrett DA, Maricevich MA, et al. (2009) Intraductal papillary mucinous neoplasm of the biliary tract: a real disease? HPB 11(8):684–691. doi:10.1111/j.1477-2574.2009.00122.x
20. Choi BI, Lee JM, Han JK (2004) Imaging of intrahepatic and hilar cholangiocarcinoma. Abdom Imaging 29(5):548–557. doi:10.1007/s00261-004-0188-1
21. Worawattanakul S, Semelka RC, Noone TC, et al. (1998) Cholangiocarcinoma: spectrum of appearances on MR images using current techniques. Magn Reson Imaging 16(9):993–1003
22. Jarnagin WR (2000) Cholangiocarcinoma of the extrahepatic bile ducts. Semin Surg Oncol 19(2):156–176
23. Edmondson HA (1956) Differential diagnosis of tumors and tumor-like lesions of liver in infancy and childhood. Am J Dis Child 91(2):168–186
24. Stipa F, Yoon SS, Liau KH, et al. (2006) Outcome of patients with fibrolamellar hepatocellular carcinoma. Cancer 106(6):1331–1338. doi:10.1002/cncr.21703
25. Ichikawa T, Federle MP, Grazioli L, et al. (1999) Fibrolamellar hepatocellular carcinoma: imaging and pathologic findings in 31 recent cases. Radiology 213(2):352–361. doi:10.1148/radiology.213.2.r99nv31352
26. Ganeshan D, Szklaruk J, Kundra V, et al. (2014) Imaging features of fibrolamellar hepatocellular carcinoma. Am J Roentgenol 202(3):544–552. doi:10.2214/AJR.13.11117
27. McLarney JK, Rucker PT, Bender GN, et al. (1999) Fibrolamellar carcinoma of the liver: radiologic-pathologic correlation. Radiographics 19(2):453–471. doi:10.1148/radiographics.19.2.g99mr09453
28. Smith MT, Blatt ER, Jedlicka P, Strain JD, Fenton LZ (2008) Best cases from the AFIP: fibrolamellar hepatocellular carcinoma. Radiographics 28(2):609–613. doi:10.1148/rg.282075153
29. El-Serag HB, Davila JA (2004) Is fibrolamellar carcinoma different from hepatocellular carcinoma? A US population-based study. Hepatology 39(3):798–803. doi:10.1002/hep.20096
30. Liu S, Chan KW, Wang B, Qiao L (2009) Fibrolamellar hepatocellular carcinoma. Am J Gastroenterol 104(10):2617–2624 ((quiz 2625)). doi:10.1038/ajg.2009.440
31. Steiner PE, Higginson J (1959) Cholangiolocellular carcinoma of the liver. Cancer 12(4):753–759
32. Asayama Y, Tajima T, Okamoto D, et al. (2010) Imaging of cholangiolocellular carcinoma of the liver. Eur J Radiol 75(1):e120–e125. doi:10.1016/j.ejrad.2009.09.010
33. Allen RA, Lisa JR (1949) Combined liver cell and bile duct carcinoma. Am J Pathol 25(4):647–655
34. Joo I, Lee JM (2013) Imaging bile duct tumors: pathologic concepts, classification, and early tumor detection. Abdom Imaging 38(6):1334–1350. doi:10.1007/s00261-013-0027-3
35. Motosugi U, Ichikawa T, Nakajima H, et al. (2009) Cholangiolocellular carcinoma of the liver: imaging findings. J Comput Assist Tomogr 33(5):682–688. doi:10.1097/RCT.0b013e318195400c
36. de Campos RO, Semelka RC, Azevedo RM, et al. (2012) Combined hepatocellular carcinoma-cholangiocarcinoma: report of MR appearance in eleven patients. J Magn Reson Imaging 36(5):1139–1147. doi:10.1002/jmri.23754
37. Riopel MA, Klimstra DS, Godellas CV, Blumgart LH, Westra WH (1997) Intrabiliary growth of metastatic colonic adenocarcinoma: a pattern of intrahepatic spread easily confused with primary neoplasia of the biliary tract. Am J Surg Pathol 21(9):1030–1036

38. Wenzel DJ, Gaede JT, Wenzel LR (2003) Case report. Intrabiliary colonic metastasis mimicking primary biliary neoplasia. Am J Roentgenol 180(4):1029–1032. doi:10.2214/ajr.180.4.1801029
39. Povoski SP, Klimstra DS, Brown KT, et al. (2000) Recognition of intrabiliary hepatic metastases from colorectal adenocarcinoma. HPB Surg 11(6):383–390 ((discussion 390–381))
40. Herbut PA, Watson JS (1946) Metastatic cancer of the extrahepatic bile ducts producing jaundice. Am J Clin Pathol 16(6): 365–372
41. Peungjesada S, Aloia TA, Kaur H, et al. (2013) Intrabiliary growth of colorectal liver metastasis: spectrum of imaging findings and implications for surgical management. Am J Roentgenol 201(4):W582–W589. doi:10.2214/AJR.12.9508
42. Okano K, Yamamoto J, Okabayashi T, et al. (2002) CT imaging of intrabiliary growth of colorectal liver metastases: a comparison of pathological findings of resected specimens. Br J Radiol 75(894):497–501
43. Tokai H, Kawashita Y, Eguchi S, et al. (2006) A case of mucin producing liver metastases with intrabiliary extension. World J Gastroenterol 12(30):4918–4921
44. Eliason SC, Grosso LE (2001) Primary biliary malignant lymphoma clinically mimicking cholangiocarcinoma: a case report and review of the literature. Ann Diagn Pathol 5(1):25–33. doi: 10.1053/adpa.2001.21483
45. Nguyen GK (1982) Primary extranodal non-Hodgkin's lymphoma of the extrahepatic bile ducts. Report of a case. Cancer 50(10): 2218–2222
46. Lei KI (1998) Primary non-Hodgkin's lymphoma of the liver. Leuk Lymphoma 29(3–4):293–299. doi:10.3109/10428199809068566
47. Gaulard P, Zafrani ES, Mavier P, et al. (1986) Peripheral T-cell lymphoma presenting as predominant liver disease: a report of three cases. Hepatology 6(5):864–868
48. Das K, Fisher A, Wilson DJ, et al. (2003) Primary non-Hodgkin's lymphoma of the bile ducts mimicking cholangiocarcinoma. Surgery 134(3):496–500
49. Ohtomo K, Baron RL, Dodd GD III, et al. (1993) Confluent hepatic fibrosis in advanced cirrhosis: evaluation with MR imaging. Radiology 189(3):871–874. doi:10.1148/radiology.189.3.8234718
50. Campos JT, Sirlin CB, Choi JY (2012) Focal hepatic lesions in Gd-EOB-DTPA enhanced MRI: the atlas. Insights Imaging 3(5):451–474. doi:10.1007/s13244-012-0179-7
51. Brancatelli G, Baron RL, Federle MP, Sparacia G, Pealer K (2009) Focal confluent fibrosis in cirrhotic liver: natural history studied with serial CT. Am J Roentgenol 192(5):1341–1347. doi: 10.2214/AJR.07.2782
52. Patankar T, Prasad S, Shenoy A, Rathod K (2000) Pulmonary inflammatory pseudotumour in children. Australas Radiol 44(3): 318–320
53. Tang L, Lai EC, Cong WM, et al. (2010) Inflammatory myofibroblastic tumor of the liver: a cohort study. World J Surg 34(2):309–313. doi:10.1007/s00268-009-0330-x
54. Pack GT, Baker HW (1953) Total right hepatic lobectomy; report of a case. Ann Surg 138(2):253–258
55. Faraj W, Ajouz H, Mukherji D, et al. (2011) Inflammatory pseudo-tumor of the liver: a rare pathological entity. World J Surg Oncol 9:5. doi:10.1186/1477-7819-9-5
56. Yoon KH, Ha HK, Lee JS, et al. (1999) Inflammatory pseudotumor of the liver in patients with recurrent pyogenic cholangitis: CT-histopathologic correlation. Radiology 211(2):373–379. doi: 10.1148/radiology.211.2.r99ma36373
57. Menias CO, Surabhi VR, Prasad SR, et al. (2008) Mimics of cholangiocarcinoma: spectrum of disease. Radiographics 28(4): 1115–1129. doi:10.1148/rg.284075148
58. Narla LD, Newman B, Spottswood SS, Narla S, Kolli R (2003) Inflammatory pseudotumor. Radiographics 23(3):719–729. doi: 10.1148/rg.233025073
59. Patnana M, Sevrukov AB, Elsayes KM, et al. (2012) Inflammatory pseudotumor: the great mimicker. Am J Roentgenol 198(3): W217–W227. doi:10.2214/AJR.11.7288
60. Pollock AN, Newman B, Putnam PE, Dickman PS, Medina JL (1995) Imaging of post-transplant spindle cell tumors. Pediatr Radiol 25(Suppl 1):S118–S121
61. Kitajima K, Shiba H, Nojiri T, et al. (2007) Intrahepatic cholangiocarcinoma mimicking hepatic inflammatory pseudotumor. J Gastrointest Surg 11(3):398–402. doi:10.1007/s11605-006-0071-1
62. Nonomura A, Minato H, Shimizu K, Kadoya M, Matsui O (1997) Hepatic hilar inflammatory pseudotumor mimicking cholangiocarcinoma with cholangitis and phlebitis—a variant of primary sclerosing cholangitis? Pathol Res Pract 193(7):519–525 ((discussion 526)). doi:10.1016/S0344-0338(97)80106-9
63. Sarrami AH, Baradaran-Mahdavi MM, Meidani M (2012) Precise recognition of liver inflammatory pseudotumor may prevent an unnecessary surgery. Int J Prev Med 3(6):432–434
64. Doerr W (1956) Lympnepithelial Schmincke-Regaud tumors. Arztl Wochensch 11(8–9):169–182
65. Kim YC, Park MS, Chung YE, et al. (2010) MRI findings of uncommon non-hepatocyte origin primary liver tumours with pathological correlation. Br J Radiol 83(996):1080–1086. doi: 10.1259/bjr/61140265
66. Shinoda M, Kadota Y, Tsujikawa H, et al. (2013) Lymphoepithelioma-like hepatocellular carcinoma: a case report and a review of the literature. World J Surg Oncol 11:97. doi:10.1186/1477-7819-11-97
67. Nemolato S, Fanni D, Naccarato AG, et al. (2008) Lymphoepitelioma-like hepatocellular carcinoma: a case report and a review of the literature. World J Gastroenterol 14(29):4694–4696
68. Shirabe K, Matsumata T, Maeda T, et al. (1995) A long-term surviving patient with hepatocellular carcinoma including lymphocytes infiltration—a clinicopathological study. Hepatogastroenterology 42(6):996–1001
69. Min HS, Shin E, Jang JJ (2007) Carcinoma with predominant lymphoid stroma in hepatobiliary system—report of 2 cases. Korean J Hepatol 13(2):222–227
70. Emile JF, Adam R, Sebagh M, et al. (2000) Hepatocellular carcinoma with lymphoid stroma: a tumour with good prognosis after liver transplantation. Histopathology 37(6):523–529
71. LaRusso NF, Shneider BL, Black D, et al. (2006) Primary sclerosing cholangitis: summary of a workshop. Hepatology 44(3): 746–764. doi:10.1002/hep.21337
72. Burak K, Angulo P, Pasha TM, et al. (2004) Incidence and risk factors for cholangiocarcinoma in primary sclerosing cholangitis. Am J Gastroenterol 99(3):523–526. doi:10.1111/j.1572-0241.2004.04067.x
73. Moreno Luna LE, Gores GJ (2006) Advances in the diagnosis of cholangiocarcinoma in patients with primary sclerosing cholangitis. Liver Transpl 12(11 Suppl 2):S15–S19. doi:10.1002/lt.20938
74. Broome U, Lofberg R, Veress B, Eriksson LS (1995) Primary sclerosing cholangitis and ulcerative colitis: evidence for increased neoplastic potential. Hepatology 22(5):1404–1408
75. Soetikno RM, Lin OS, Heidenreich PA, Young HS, Blackstone MO (2002) Increased risk of colorectal neoplasia in patients with primary sclerosing cholangitis and ulcerative colitis: a meta-analysis. Gastrointest Endosc 56(1):48–54
76. Weber C, Kuhlencordt R, Grotelueschen R, et al. (2008) Magnetic resonance cholangiopancreatography in the diagnosis of primary sclerosing cholangitis. Endoscopy 40(9):739–745. doi:10.1055/s-2008-1077509
77. Maggs JR, Chapman RW (2008) An update on primary sclerosing cholangitis. Curr Opin Gastroenterol 24(3):377–383. doi:10.1097/MOG.0b013e3282f9e239
78. Mendes F, Lindor KD (2010) Primary sclerosing cholangitis: overview and update. Nat Rev Gastroenterol Hepatol 7(11):611–619. doi:10.1038/nrgastro.2010.155
79. Textor HJ, Flacke S, Pauleit D, et al. (2002) Three-dimensional magnetic resonance cholangiopancreatography with respiratory triggering in the diagnosis of primary sclerosing cholangitis: comparison with endoscopic retrograde cholangiography. Endoscopy 34(12):984–990. doi:10.1055/s-2002-35830
80. Chapman R, Fevery J, Kalloo A, et al. (2010) Diagnosis and management of primary sclerosing cholangitis. Hepatology 51(2): 660–678. doi:10.1002/hep.23294
81. Campbell WL, Ferris JV, Holbert BL, Thaete FL, Baron RL (1998) Biliary tract carcinoma complicating primary sclerosing cholangitis: evaluation with CT, cholangiography, US, and MR imaging. Radiology 207(1):41–50. doi:10.1148/radiology.207.1.9530297

82. Abdalian R, Heathcote EJ (2006) Sclerosing cholangitis: a focus on secondary causes. Hepatology 44(5):1063–1074. doi:10.1002/hep.21405
83. Benhamou Y, Caumes E, Gerosa Y, et al. (1993) AIDS-related cholangiopathy. Critical analysis of a prospective series of 26 patients. Dig Dis Sci 38(6):1113–1118
84. Tonolini M, Bianco R (2013) HIV-related/AIDS cholangiopathy: pictorial review with emphasis on MRCP findings and differential diagnosis. Clin Imaging 37(2):219–226. doi:10.1016/j.clinimag.2012.03.008
85. Bilgin M, Balci NC, Erdogan A, et al. (2008) Hepatobiliary and pancreatic MRI and MRCP findings in patients with HIV infection. Am J Roentgenol 191(1):228–232. doi:10.2214/AJR.07.3197
86. Cello JP (1989) Acquired immunodeficiency syndrome cholangiopathy: spectrum of disease. Am J Med 86(5):539–546
87. Park MS, Yu JS, Kim KW, et al. (2001) Recurrent pyogenic cholangitis: comparison between MR cholangiography and direct cholangiography. Radiology 220(3):677–682. doi:10.1148/radiol.2202001252
88. Knowlton JQ, Taylor AJ, Reichelderfer M, Stang J (2008) Imaging of biliary tract inflammation: an update. Am J Roentgenol 190(4):984–992. doi:10.2214/AJR.07.3033
89. Kruskal JB, Kane RA (2001) Intraoperative sonography of the biliary system. Am J Roentgenol 177(2):395–403. doi:10.2214/ajr.177.2.1770395
90. Hamano H, Kawa S, Horiuchi A, et al. (2001) High serum IgG4 concentrations in patients with sclerosing pancreatitis. N Engl J Med 344(10):732–738. doi:10.1056/NEJM200103083441005
91. Hirano K, Komatsu Y, Yamamoto N, et al. (2004) Pancreatic mass lesions associated with raised concentration of IgG4. Am J Gastroenterol 99(10):2038–2040. doi:10.1111/j.1572-0241.2004.40215.x
92. Kawaguchi K, Koike M, Tsuruta K, et al. (1991) Lymphoplasmacytic sclerosing pancreatitis with cholangitis: a variant of primary sclerosing cholangitis extensively involving pancreas. Hum Pathol 22(4):387–395
93. Okazaki K, Uchida K, Chiba T (2001) Recent concept of autoimmune-related pancreatitis. J Gastroenterol 36(5):293–302
94. Sahani DV, Kalva SP, Farrell J, et al. (2004) Autoimmune pancreatitis: imaging features. Radiology 233(2):345–352. doi:10.1148/radiol.2332031436
95. Nakazawa T, Ohara H, Sano H, Ando T, Joh T (2006) Schematic classification of sclerosing cholangitis with autoimmune pancreatitis by cholangiography. Pancreas 32(2):229. doi:10.1097/01.mpa.0000202941.85955.07
96. Deltenre P, Valla DC (2006) Ischemic cholangiopathy. J Hepatol 44(4):806–817. doi:10.1016/j.jhep.2006.01.009
97. Ruemmele P, Hofstaedter F, Gelbmann CM (2009) Secondary sclerosing cholangitis. Nat Rev Gastroenterol Hepatol 6(5):287–295. doi:10.1038/nrgastro.2009.46
98. Alazmi WM, McHenry L, Watkins JL, et al. (2006) Chemotherapy-induced sclerosing cholangitis: long-term response to endoscopic therapy. J Clin Gastroenterol 40(4):353–357. doi:10.1097/01.mcg.0000210098.28876.66
99. Northover JM, Terblanche J (1979) A new look at the arterial supply of the bile duct in man and its surgical implications. Br J Surg 66(6):379–384
100. Martin RF, Rossi RL (1994) Bile duct injuries. Spectrum, mechanisms of injury, and their prevention. Surg Clin North Am 74(4):781–803 ((discussion 805–787))
101. Moser AJ (2001) Benign biliary strictures. Curr Treat Options Gastroenterol 4(5):377–387
102. Pitt HA, Kaufman SL, Coleman J, White RI, Cameron JL (1989) Benign postoperative biliary strictures. Operate or dilate? Ann Surg 210(4):417–425 ((discussion 426–417))
103. Khalid TR, Casillas VJ, Montalvo BM, Centeno R, Levi JU (2001) Using MR cholangiopancreatography to evaluate iatrogenic bile duct injury. Am J Roentgenol 177(6):1347–1352. doi:10.2214/ajr.177.6.1771347
104. Girometti R, Brondani G, Cereser L, et al. (2010) Post-cholecystectomy syndrome: spectrum of biliary findings at magnetic resonance cholangiopancreatography. Br J Radiol 83(988):351–361. doi:10.1259/bjr/99865290
105. Keleman AM, Imagawa DK, Findeiss L, et al. (2011) Associated vascular injury in patients with bile duct injury during cholecystectomy. Am Surg 77(10):1330–1333
106. Stewart L, Robinson TN, Lee CM, et al. (2004) Right hepatic artery injury associated with laparoscopic bile duct injury: incidence, mechanism, and consequences. J Gastrointest Surg 8(5):523–530 ((discussion 530–521)). doi:10.1016/j.gassur.2004.02.010
107. Shanbhogue AK, Tirumani SH, Prasad SR, Fasih N, McInnes M (2011) Benign biliary strictures: a current comprehensive clinical and imaging review. Am J Roentgenol 197(2):W295–W306. doi:10.2214/AJR.10.6002
108. Yamaguchi K, Enjoji M (1987) Carcinoma of the ampulla of vater. A clinicopathologic study and pathologic staging of 109 cases of carcinoma and 5 cases of adenoma. Cancer 59(3):506–515
109. Kim JH, Kim MJ, Chung JJ, et al. (2002) Differential diagnosis of periampullary carcinomas at MR imaging. Radiographics 22(6):1335–1352. doi:10.1148/rg.226025060
110. Semelka RC, Kelekis NL, John G, et al. (1997) Ampullary carcinoma: demonstration by current MR techniques. J Magn Reson Imaging 7(1):153–156
111. Khan MR, Ur Rehman S (2012) Mirizzi's syndrome masquerading as cholangiocarcinoma: a case report. J Med Case Rep 6(1):157. doi:10.1186/1752-1947-6-157
112. Choi BW, Kim MJ, Chung JJ, et al. (2000) Radiologic findings of Mirizzi syndrome with emphasis on MRI. Yonsei Med J 41(1):144–146
113. Ringe KI, Husarik DB, Sirlin CB, Merkle EM (2010) Gadoxetate disodium-enhanced MRI of the liver: part 1, protocol optimization and lesion appearance in the noncirrhotic liver. Am J Roentgenol 195(1):13–28. doi:10.2214/AJR.10.4392
114. Lee NK, Kim S, Kim GH, et al. (2012) Diffusion-weighted imaging of biliopancreatic disorders: correlation with conventional magnetic resonance imaging. World J Gastroenterol 18(31):4102–4117. doi:10.3748/wjg.v18.i31.4102
115. Kim JY, et al. (2007) Contrast-enhanced MRI combined with MR cholangiopancreatography for the evaluation of patients with biliary strictures: differentiation of malignant from benign bile duct strictures. J Magn Reson Imaging 26(2):304–312